

SA²GFM: Enhancing Robust Graph Foundation Models with Structure-Aware Semantic Augmentation

Junhua Shi¹, Qingyun Sun^{1*}, Haonan Yuan¹, Xingcheng Fu²

¹SKLCCSE, School of Computer Science and Engineering, Beihang University, Beijing, China

²Key Lab of Education Blockchain and Intelligent Technology, Guangxi Normal University, Guilin, China
 {shijunhua, sunqy, yuanhn}@buaa.edu.cn, fuxc@gxnu.edu.cn

Abstract

While Graph Foundation Models (GFMs) have achieved notable progress across diverse tasks recently, their robustness under domain noise, structural perturbations, and even adversarial attacks remains largely underexplored. A core limitation lies in the inadequate modeling of hierarchical structural semantics, which are intrinsic priors and critical for generalization. In this work, we propose SA²GFM, a robust GFM framework that enhances the domain-adaptable representations through Structure-Aware Semantic Augmentation. First, to embed the hierarchical structural priors, we transform entropy-based encoding trees into structure-aware textual prompts for feature augmentation. The enriched inputs are processed by a novel self-supervised Information Bottleneck mechanism that distills the robust and transferable representations through structure-guided compression. To mitigate the negative transfer in cross-domain adaptation, we develop an expert adaptive routing mechanism that integrates a mixture-of-experts architecture with a null expert design. To enable efficient downstream adaptation, we propose a fine-tuning module that efficiently optimizes the hierarchical structures through the joint intra- and inter-community structure learning. Extensive experiments validate the superiority of SA²GFM over effectiveness and robustness against random noise and adversarial perturbations on node and graph classification compared with 9 state-of-the-art baselines.

1 Introduction

Graph Neural Networks (GNNs) have achieved impressive success in learning graph-structured data (Kipf and Welling 2017; Veličković et al. 2018) across a wide range of domains. However, traditional GNNs are designed for specific tasks and datasets, limiting their ability to transfer learned knowledge to unseen domains (Hu et al. 2020b). To address this limitation, recent work has advanced towards Graph Foundation Models (GFMs), which aim to learn general-purpose graph representations via large-scale multi-domain pre-training and efficient downstream adaptation with limited supervision (Yu et al. 2024; Wang et al. 2025; Yuan et al. 2025b). The paradigm of “pretrain-then-finetune” promises to build adaptable GFMs that generalize across a broad spectrum of graph-based tasks and domains (Liu et al. 2023a).

*Corresponding author.

Copyright © 2026, Association for the Advancement of Artificial Intelligence (www.aaai.org). All rights reserved.

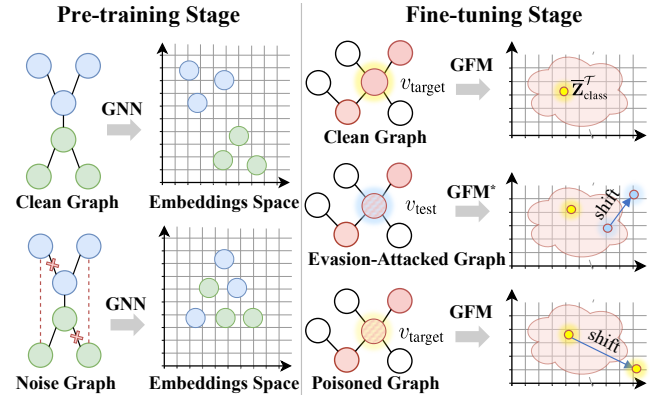


Figure 1: Effects of different attacks in pre-training and fine-tuning. The asterisk (*) denotes the trained module.

As shown in Figure 1, the robustness of Graph Foundation Models (GFMs) under noisy and adversarial perturbations remains largely underexplored (Wang et al. 2025). Particularly, a fundamental limitation arises from the insufficient modeling of hierarchical structural semantics: the inductive priors that are crucial for ensuring both adaptation and robustness. Existing GFMs predominantly adopt shallow message-passing GNNs as their backbone architectures, which are theoretically limited by the 1-Weisfeiler-Lehman (1-WL) test (Xu et al. 2019; Morris et al. 2019), rendering them incapable of distinguishing structurally similar yet semantically distinct patterns. Consequently, their learned representations often neglect long-range dependencies and higher-order structure semantics, leaving them vulnerable to noise and misalignment under real-world deployment. Moreover, most GFMs overlook the opportunity to embed structure-aware semantics (Yu et al. 2024; Yuan et al. 2025b). They tend to directly encode raw node attributes, which are often incomplete or noisy, while ignoring global community hierarchies that provide stable semantic anchors across domains. Without explicit modeling of such structure-induced semantics.

Beyond architectural expressiveness, GFMs often struggle in real-world deployment where robustness is essential. Existing domain adaptation GFMs (e.g., MDGPT (Yu et al. 2024), BRIDGE) (Yuan et al. 2025b) rely on over-idealized

assumptions like dimension alignment or domain invariance, which frequently break across heterogeneous graphs (Wang et al. 2024). Meanwhile, some other GFMs claim to be perturbation robust by applying global structure learning (Wang et al. 2025), but they often incur high computational costs and remain fragile to localized perturbations or adversarial attacks (Kataria, Kumar, and Jayadeva 2024; Zhang et al. 2024). A more critical yet overlooked problem is negative transfer: when structural or semantic gaps between domains are large, the naïve source aggregation can severely degrade downstream performance, especially under dynamic or non-stationary settings (Dan et al. 2024; Yuan et al. 2023).

The aforementioned challenges expose three critical bottlenecks for constructing a robust GFM: (1) **Pre-training: How to embed structural semantic priors while preserving information purity?** Raw node features are insufficient for capturing transferable patterns across domains, yet naïve feature enhancement may introduce spurious correlations. A principled mechanism is needed to embed high-level structural priors while compressing irrelevant noise. (2) **Knowledge fusion: How to mitigate negative transfer under domain discrepancy?** The diverse nature of real-world graphs necessitates adaptive fusion strategies that can selectively route relevant knowledge and suppress misleading signals from unrelated sources. (3) **Downstream fine-tuning: How to efficiently optimize structures under noise and adversarial perturbations?** Topology is the most vulnerable aspect of graphs, yet precise and efficient structure refinement remains an open problem due to the high cost and fragility of global structure learning strategies.

To address the challenges, we propose a novel **SA²GFM**, a robust **Graph Foundation Model** empowered by **Structure-Aware Semantic Augmentation**. Our key insight is to embed hierarchical semantic priors using entropy-based encoding trees, which generate structure-aware prompts to enrich node features. The augmented inputs are processed by a self-supervised Information Bottleneck mechanism to learn robust, domain-adaptable representations by compressing redundancy and preserving label-relevant information. To mitigate domain mismatch, we adopt an expert routing module with a Mixture-of-Experts and a null expert to suppress irrelevant sources. Finally, a lightweight fine-tuning strategy refines graph structures through hierarchical optimization for improved robustness. **Our contributions are:**

- We propose SA²GFM, a robust GFM framework by synergistically addressing key interrelated challenges in feature enhancement, principled and efficient structure optimization, and knowledge fusion.
- It integrates a structure-aware pre-training strategy utilizing encoding tree textual prompts and self-supervised Information Bottleneck, a domain-adaptive MoE with a null expert for transfer mitigation, and an efficient fine-tuning module for hierarchical structure refinement.
- Extensive experiments show superiority of SA²GFM over effectiveness and robustness against noise and adversarial perturbations on node and graph classification compared with 9 state-of-the-art baselines.

2 Related Work

Detailed related works are discussed in Appendix E.

2.1 Multi-domain Graph Foundation Models

Multi-domain pre-training is fundamental for constructing graph foundation models capable of adapting across heterogeneous graphs (Yuan et al. 2025c,a). Existing methods typically align either node features, using domain tokens (Yu et al. 2024) or domain-invariant aligners (Yuan et al. 2025b), or graph structures via Graph Structure Learning (GSL) (Wang et al. 2025). Some approaches also explore flexible transfer frameworks to reduce negative transfer (Ju et al. 2025). However, most of these efforts address feature and structure adaptation in isolation, lacking a unified perspective that jointly considers both levels.

2.2 Robust Graph Representation Learning

The line of research aims to improve stability under feature and structure noise. For feature robustness, prior work leverages data augmentation (Zheng, Wang, and Liu 2024; Huang et al. 2025) and adversarial training (Lee and Park 2025). For structural robustness, Graph Structure Learning (GSL) is widely used to counter topological perturbations (Zügner, Akbarnejad, and Günnemann 2018; Yuan et al. 2024). However, most methods treat feature and structure separately, and many GSL techniques remain costly and coarse-grained.

2.3 Graph Structural Entropy

Graph Structural Entropy is an information-theoretic measure that captures the hierarchical organization of a graph through community encoding (Li and Pan 2016). This hierarchy has shown promise in guiding representation learning (Bai et al. 2024), yet its use for enhancing raw node features and improving the robustness of graph foundation models remains largely unexplored.

3 Preliminary

Notations. A graph is denoted as $G = (\mathcal{V}, \mathcal{E})$, where \mathcal{V} is the node set and \mathcal{E} is the edge set. Let $\mathbf{A} \in \{0, 1\}^{N \times N}$ be the adjacency matrix and $\mathbf{X} \in \mathbb{R}^{N \times d_i}$ be the node feature matrix, where $N = |\mathcal{V}|$ is the number of nodes and d_i denotes input dimension. \mathbf{Z} is hidden embeddings of \mathbf{X} .

Problem Settings. Our proposed SA²GFM operates under the multi-domain pre-training and few-shot fine-tuning paradigm. Given n source graphs $\{G^S\} \in \mathcal{G}^S$ from multiple domains $\{D^S\} \in \mathcal{D}^S$ with their labels $\{Y^S\} \in \mathcal{Y}^S$, the pre-training goal is to train a graph learner $h = g(\mathcal{F}_\Theta(\cdot))$ on multi-domain graph datasets, after which the pre-training parameter Θ^* is frozen. During fine-tuning, given a set of target graphs $\{G^T\} \in \mathcal{G}^T$ (potentially corrupted by noise or adversarial attacks) from target domain $\{D^T\} \in \mathcal{D}^T$ (seen or unseen) with m accessible labels $\{Y^T\} \in \mathcal{Y}^T$ under m -shot setting ($m \ll n$), the ultimate goal is to leverage the pre-trained Θ^* to achieve robust performance on the unlabeled nodes of the target graph.

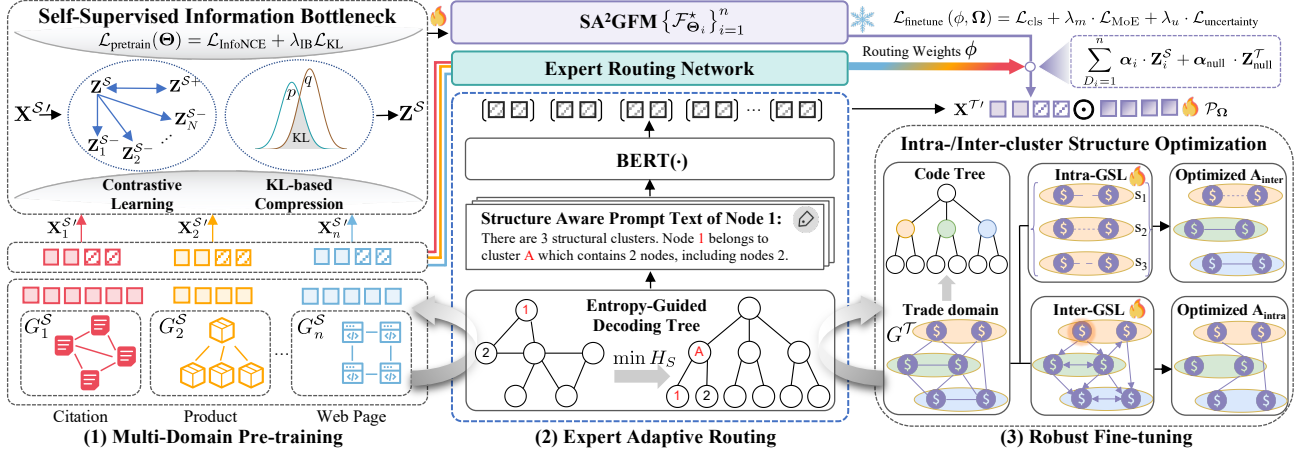


Figure 2: Overview of the SA²GFM framework. The framework first pre-trains an ensemble of expert encoders on multiple source domains using Structure-Aware Semantic Augmentation and an Information Bottleneck objective. During fine-tuning, a novel Expert Adaptive Routing mechanism selects knowledge to mitigate negative transfer, while a Hierarchical Structure Optimization module refines the target graph’s topology before final prediction.

4 Proposed Framework: SA²GFM

In this section, we introduce the proposed SA²GFM with its framework illustrated in Figure 2.

4.1 Multi-domain Pre-training with Self-Supervised Information Bottleneck

We begin by encoding structural priors into node features via textual prompts derived from entropy-based encoding trees.

Structure-Aware Semantic Augmentation. Real-world graphs exhibit rich hierarchical priors that are not explicitly encoded in node. To expose such a structure to encoders, we propose to convert the latent community hierarchy into textual prompts, which allows the pre-trained language models to serve as a bridge between structural regularities and semantic representations. To achieve this, we leverage the theory of graph structural entropy (Long et al. 2020), which identifies an optimal recursive clustering by minimizing entropy over volume-weighted partitions. Given a partition $\mathcal{C}^S = \{C_1, \dots, C_K\}$ of graph G^S , the entropy is:

$$H_S(G^S) = - \sum_{k=1}^K \frac{\text{Vol}(C_k)}{\text{Vol}(G^S)} \log \frac{\text{Vol}(C_k)}{\text{Vol}(G^S)}, \quad (1)$$

where $\text{Vol}(C_k)$ represents the sum of degrees in cluster C_k . Based on this tree, we construct a structured textual prompt \mathbf{t}_i for node v_i that captures its structural role, such as: “*There are K structural clusters. Node v_i belongs to cluster C_k , which contains N_k nodes, including v_i, \dots, v_j .*” As shown in Figure 3, the encoding tree guides prompt generation by selecting a node’s local cluster, identifying its peer nodes, and transforming this information into language models. This prompt is then embedded via BERT and fused:

$$\mathbf{x}_i^{S'} = \text{SVD}(\mathbf{x}_i^S) \oplus \text{SVD}(\text{BERT}(\mathbf{t}_i)), \quad (2)$$

where $\text{SVD}(\cdot)$ is implemented by truncated SVD (Stewart 1993) that aligns feature dimensions as d_0 .

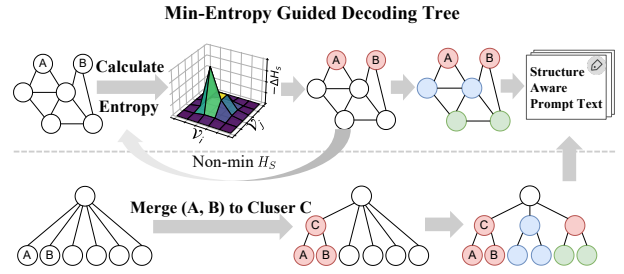


Figure 3: Construct code tree by minimizing structure entropy to generate structure aware prompt text.

Self-Supervised Information Bottleneck. Given aligned features $\mathbf{X}^{S'}$, our goal is to learn the robust and compressed representations $\mathbf{Z}^S = \mathcal{F}_{\Theta}(\mathbf{X}^{S'}, \mathbf{A}^S) \in \mathbb{R}^d$ that retain task-relevant semantics while suppressing noise. Following the Information Bottleneck (IB) principle (Tishby, Pereira, and Bialek 1999), we formulate a self-supervised objective to maximize consistency between similar nodes while compressing redundant input information. Formally, we define the self-supervised IB (SS-IB) objective as:

$$\mathcal{L}_{\text{SS-IB}} = -I(\mathbf{Z}^S; \mathbf{Z}^{S'}) + \beta \cdot I(\mathbf{Z}^S; \mathbf{X}^{S'}), \quad (3)$$

where the prediction term $I(\mathbf{Z}^S; \mathbf{Z}^{S'})$ maximizes consistency between an anchor \mathbf{Z}^S and its positive sample $\mathbf{Z}^{S'}$, which is sampled from its structural neighborhood based on the encoding tree. The compression term $I(\mathbf{Z}^S; \mathbf{X}^{S'})$ enforces compression by limiting the information retained from the input $\mathbf{X}^{S'}$. β is a balancing hyperparameter.

As directly optimizing Eq. (3) is generally intractable, we adopt variational bounds to implement $\mathcal{L}_{\text{SS-IB}}$.

Derivation 1 (Lower Bound of $I(\mathbf{Z}^S; \mathbf{Z}^{S'})$). Prediction term $I(\mathbf{Z}^S; \mathbf{Z}^{S'})$ is lower-bounded by InfoNCE (Oord, Li, and Vinyals 2018). For each anchor v_i and positive node v_i^+ :

$$\begin{aligned} I(\mathbf{Z}^S; \mathbf{Z}^{S+}) &\geq -\mathcal{L}_{\text{InfoNCE}} \\ &= \frac{1}{N^+} \sum_{i=1}^{N^+} \log \frac{\exp(\langle \mathbf{Z}_i^S, \mathbf{Z}_i^{S+} \rangle / \tau)}{\sum_{j=0}^{N^-} \exp(\langle \mathbf{Z}_i^S, \mathbf{Z}_j^S \rangle / \tau)}, \end{aligned} \quad (4)$$

where N^+ and N^- are the number of positive and negative samples, which are non-redundantly and consistently sampled from the source domain depending on whether there is a direct link (Liu et al. 2023b). τ is a temperature.

Derivation 2 (Upper Bound of $I(\mathbf{Z}^S; \mathbf{X}^{S'})$). Compression term $I(\mathbf{Z}^S; \mathbf{X}^{S'})$ is upper-bounded by the KL divergence between posterior $q(\mathbf{Z}^S | \mathbf{X}^{S'})$ and prior $p(\mathbf{Z}^S)$:

$$I(\mathbf{Z}^S; \mathbf{X}^{S'}) \leq \frac{1}{N} \sum_{i=1}^N \text{KL}[q(\mathbf{Z}_i^S | \mathbf{X}_i^{S'}) \| p(\mathbf{Z}_i^S)], \quad (5)$$

We assume a standard Gaussian prior $p(\mathbf{Z}^S) = \mathcal{N}(\mathbf{0}, \mathbf{I})$, and apply the graph encoder to produce the mean $\boldsymbol{\mu}_i$ and the log-variance $\log \boldsymbol{\sigma}_i^2$ of $q(\mathbf{Z}_i^S | \mathbf{X}_i^{S'})$ for each node v_i , from which we sample \mathbf{Z}_i^S via reparameterization trick:

$$\mathbf{Z}_i^S \sim q(\mathbf{Z}_i^S | \mathbf{X}_j^{S'}) = \mathcal{N}(\boldsymbol{\mu}_i, \text{diag}(\boldsymbol{\sigma}_i^2)). \quad (6)$$

We provide detailed proofs in Appendix B.

Pre-training Objective. By integrating these bounds, we transform $\mathcal{L}_{\text{SS-IB}}$ in Eq. (3) into a tractable objective given n source domain graphs with trade-off coefficient λ_{IB} :

$$\mathcal{L}_{\text{pretrain}}(\Theta) = \frac{1}{n} \sum_{D_i=1}^n \mathcal{L}_{\text{InfoNCE}} + \lambda_{\text{IB}} \mathcal{L}_{\text{KL}}, \quad (7)$$

$\uparrow \text{Eq. (4)}$ $\uparrow \text{Eq. (5)}$

after which the learned Θ^* is frozen. Overall, pre-training phase leverages pre-trained language models as a bridge to transform structural priors into node features, enabling the capture of transferable knowledge that lays robust foundation for next expert routing and downstream fine-tuning.

4.2 Expert Adaptive Routing with Negative Transfer Mitigation

To prevent negative transfer, we introduce an expert adaptive routing mechanism, which not only “selects” helpful experts but also “rejects” negative ones via a learnable null expert.

Gated Routing with Null-Expert. To enable fine-grained adaptation across multiple source domains while mitigating negative transfer, we introduce a gated routing network \mathcal{R}_ϕ that dynamically modulates the contribution of each source expert from $\mathcal{F}_\Theta^* = \{f_{\Theta_1}^*, f_{\Theta_2}^*, \dots, f_{\Theta_n}^*\}$ via a learned routing weights $\boldsymbol{\alpha} = \{\boldsymbol{\alpha}_1, \dots, \boldsymbol{\alpha}_n, \boldsymbol{\alpha}_{\text{null}}\}$, where the null expert explicitly captures and suppresses irrelevant knowledge.

Specifically, we first derive prototypes for the target and source domains. Let $\bar{\mathbf{Z}}^T$ denote the mean-pooled embedding of m ($m \ll n$) few-shot supporting samples (node or graph) in the target graph(s). Similarly, let $\{\bar{\mathbf{Z}}_i^S\}_{i=1}^n$ represent the corresponding prototypes from each of the n source domains. We define the cosine similarity vector $\mathbf{S} \in \mathbb{R}^n$:

$$\mathbf{S}_i = \langle \bar{\mathbf{Z}}^T, \bar{\mathbf{Z}}_i^S \rangle / \|\bar{\mathbf{Z}}^T\| \cdot \|\bar{\mathbf{Z}}_i^S\|, \quad (8)$$

where \mathbf{S} is passed through a learnable router \mathcal{R}_ϕ , yielding the unnormalized logits for the gating distribution:

$$\boldsymbol{\alpha} = \text{Softmax}(\mathcal{R}_\phi(\mathbf{S})) \in \Delta^{n+1}, \quad (9)$$

where Δ^{n+1} is the $(n+1)$ -dimensional probability simplex. Let $\mathbf{Z}_i^S \in \mathbb{R}^{N_i \times d}$ be the node-level embeddings from the i -th expert, and let $\mathbf{Z}_{\text{null}}^T$ denote the embedding generated by a shallow GCN trained solely on the target graph. The final task-specific representation is a convex combination:

$$\mathbf{Z}_{\text{final}}^T = \sum_{D_i=1}^n \boldsymbol{\alpha}_i \cdot \mathbf{Z}_i^S + \boldsymbol{\alpha}_{\text{null}} \cdot \mathbf{Z}_{\text{null}}^T, \quad (10)$$

which enables the model to selectively integrate transferable domain knowledge, and further assign high mass to null experts when there is no source expert that aligns semantically or structurally, thus mitigating negative transfer.

Uncertainty-Aware Routing Regularization. To inspire confident expert selection and avoid the overly diffuse gating, we incorporate an entropy-based regularization over the mixture-of-experts (MoE) architecture:

$$\mathcal{L}_{\text{MoE}}(\boldsymbol{\phi}) = \mathcal{H}(\boldsymbol{\alpha}) = - \sum_{j=1}^{k+1} \boldsymbol{\alpha}_j \log \boldsymbol{\alpha}_j, \quad (11)$$

where $\mathcal{H}(\cdot)$ is the entropy. It penalizes uncertain mixtures and promotes sparse, decisive routing behaviors. In particular, when all source experts are irrelevant, this regularization amplifies the model’s preference for the null expert.

4.3 Fine-tuning with Efficient Hierarchical Structure Optimization

While expert routing has aligned the source knowledge, performance still hinges on target graphs. Potential structural noise and adversarial perturbations can greatly hinder message passing. Though structure learning improves robustness (Zügner, Akbarnejad, and Günnemann 2018; Zhu et al. 2021), it is often inefficient and coarse-grained. We thus propose a lightweight structure optimization strategy.

To ensure a seamless transition from pre-training to fine-tuning, we preserve structural consistency by reusing the entropy encoding tree to partition the target graph G^T into a set of clusters \mathcal{C}^T . This partition forms the basis for the hierarchical structure optimization during fine-tuning, enabling targeted refinement at both the intra- and inter-cluster levels. While intra-cluster optimization enhances local structural fidelity, inter-cluster optimization focuses on global signal propagation and robustness.

Intra-cluster Structure Learning. For each of cluster $c \in \mathcal{C}^T$, we refine its internal topology by refining edges with multi-head attention. Let \mathbf{Z}_c^T denote the node embedding in cluster c , which are projected to $\mathbf{H}_c = \text{ReLU}(\mathbf{Z}_c^T \mathbf{W}_p)$. Attention matrix $\mathbf{S}_{\text{attn},c}$ is computed via:

$$\mathbf{S}_{\text{attn},c} = \frac{1}{H} \sum_{h=1}^H \text{Softmax} \left(\frac{\mathbf{Q}_h \mathbf{K}_h^\top}{\sqrt{d_k}} \right), \quad (12)$$

where $\mathbf{Q}_h = \mathbf{Z}_c \mathbf{W}_h^Q$, and $\mathbf{K}_h = \mathbf{H}_c \mathbf{W}_h^K$. To enforce the cross-head consistency, we introduce an uncertainty loss that penalizes variance among heads:

$$\mathcal{L}_{\text{uncertainty}} = \frac{\sum_{c \in \mathcal{C}^T} \sum_{i,j \in c, i \neq j} \text{Var}_{h=1}^H (\mathbf{S}_{ij}^{(h)})}{|\{(i,j) | i, j \in c, c \in \mathcal{C}^T, i \neq j\}|}, \quad (13)$$

where $\text{Var}(\cdot)$ denotes variation. Refined intra-cluster $\mathbf{A}_{\text{intra},c}^{\mathcal{T}'}$ fuses the original $\mathbf{A}_c^{\mathcal{T}}$ and attention-derived scores:

$$\mathbf{A}_{\text{intra},c}^{\mathcal{T}'} = (1 - \mathbf{W}_c) \cdot \mathbf{A}_c^{\mathcal{T}} + \mathbf{W}_c \cdot \mathbf{S}_{\text{attn},c}, \quad (14)$$

where \mathbf{W}_c is a learnable fusion weight per cluster.

Inter-cluster Structure Learning. As intra-cluster learning focuses on refining dense local structures, inter-cluster learning aims to regulate potentially noisy global connections, which are critical for propagation but often include irrelevant edges. To selectively retain informative inter-cluster dependencies, we approximate personalized propagation of neural predictions (Gasteiger, Bojchevski, and Günnemann 2019) to compute a soft influence matrix:

$$\mathbf{S}^{\mathcal{T}} = (1 - \alpha) \cdot \sum_{t=0}^T (\alpha \cdot \tilde{\mathbf{A}}^{\mathcal{T}})^t, \quad (15)$$

where $\tilde{\mathbf{A}}^{\mathcal{T}}$ is normalized adjacency. We then derive a probabilistic pruning mask via thresholded activation to refine the original inter-cluster structure $\mathbf{A}_{\text{inter}}^{\mathcal{T}}$:

$$\mathbf{A}_{\text{inter}}^{\mathcal{T}'} = \mathbf{A}_{\text{inter}}^{\mathcal{T}} \odot \mathbf{P}^{\mathcal{T}}, \quad \mathbf{P}^{\mathcal{T}} = \sigma(\mathbf{S}^{\mathcal{T}} - \theta_{\text{thres}}), \quad (16)$$

where σ is the Sigmoid and θ_{thres} is a learnable threshold. Let $\mathbf{A}_{\text{intra, full}}^{\mathcal{T}'}$ be the block-diagonal matrix formed by assembling the refined intra-cluster matrices $\{\mathbf{A}_{\text{intra},c}^{\mathcal{T}'}\}_{c \in \mathcal{C}^{\mathcal{T}}}$. Optimized $\mathbf{A}^{\mathcal{T}'}$ for target graph is then an adaptive combination:

$$\mathbf{A}^{\mathcal{T}'} = \mathbf{W}_s \cdot \mathbf{A}_{\text{intra, full}}^{\mathcal{T}'} + (1 - \mathbf{W}_s) \cdot \mathbf{A}_{\text{inter}}^{\mathcal{T}'}, \quad (17)$$

where \mathbf{W}_s is a learnable trade-off weights.

Fine-tuning with Prompted Structure. Given $\mathbf{A}^{\mathcal{T}'}$, we embed the learnable prompts to guide downstream adaptation. For each few-shot sample, the prompted embedding is:

$$\mathbf{Z}_i^{\mathcal{T}} = \mathcal{F}_{\Theta}^*(\mathcal{P}_{\Omega} \odot \mathbf{X}_i^{\mathcal{T}'}, \mathbf{A}^{\mathcal{T}'}) \in \mathbb{R}^d, \quad (18)$$

where \mathcal{P}_{Ω} is the learnable prompt and $\mathbf{X}_i^{\mathcal{T}'}$ is the feature aligned similarly as Eq. (1). To maintain consistency with the pre-training objective, we leverage a universal task template based on contrastive loss that aligns query embeddings with class prototypes under the updated structure. Given m few-shot support samples $(G_i^{\mathcal{T}}, Y_i^{\mathcal{T}})$, the objective is:

$$\mathcal{L}_{\text{cls}}(\Omega) = - \sum_{i=1}^m \log \frac{\exp(\langle \mathbf{Z}_i^{\mathcal{T}}, \bar{\mathbf{Z}}_{Y_i}^{\mathcal{T}} \rangle / \tau)}{\sum_{Y_j} \exp(\langle \mathbf{Z}_i^{\mathcal{T}}, \bar{\mathbf{Z}}_{Y_j}^{\mathcal{T}} \rangle / \tau)}, \quad (19)$$

where $\bar{\mathbf{Z}}_{Y_j}^{\mathcal{T}}$ is prototype of Y_j and $\langle \cdot, \cdot \rangle$ is the inner product. Thus, the overall fine-tuning objective is:

$$\mathcal{L}_{\text{finetune}}(\phi, \Omega) = \mathcal{L}_{\text{cls}} + \lambda_m \cdot \mathcal{L}_{\text{MoE}} + \lambda_u \cdot \mathcal{L}_{\text{uncertainty}}, \quad (20)$$

where λ_1, λ_2 are hyperparameters.

4.4 Complexity Analysis

Suppose f is an L -layer GNN. Then, the per-epoch computational complexity of the pre-training stage is $\mathcal{O}(nL|\mathcal{E}^{\mathcal{S}}|d)$, mainly arising from the SS-IB pre-training objective over n source graphs. The per-epoch complexity of the fine-tuning stage is $\mathcal{O}(nL|\mathcal{E}^{\mathcal{T}}|d + \sum_c |\mathcal{V}_c^{\mathcal{T}}|^2)$, where the main cost comes from the encoding process and intra-cluster attention (with $|\mathcal{V}_c^{\mathcal{T}}|$ denoting the number of nodes in cluster c). The overall complexity is comparable to that of baselines such as MDGPT, while the structure optimization is more efficient than MDGFM. More details can be found in Appendix A.

5 Experiment

We evaluate the proposed SA^2GFM with the following research questions:

- **RQ1:** How robust is SA^2GFM against random noise and adversarial attacks on features and structures?
- **RQ2:** How does the performance change as the intensity of noise or attack severity increases?
- **RQ3:** Which section contributes most to the performance?
- **RQ4:** How sensitive to hyperparameters fluctuation?
- **RQ5:** How well does pre-training support transferable and task-adaptive representations?

Additional settings and results are in Appendix C and D.

5.1 Experimental Settings

Datasets. To highlight multi-domain pre-training capability, we adopt **seven** benchmark datasets from **three** domains:

- **Citation:** Cora (McCallum et al. 2000), CiteSeer (Giles, Bollacker, and Lawrence 1998), PubMed (Sen et al. 2008), ogbn-arXiv (Hu et al. 2020a).
- **Products:** ogbn-Tech, ogbn-Home (Hu et al. 2020a).
- **Web Page:** Wiki-CS (Mernyei and Cangea 2020).

Dataset statistics are summarized in Table C.1.

Baselines. Include **nine** baselines from **four** categories:

- GCN (Kipf et al. 2017), GAT (Veličković et al. 2018).
- **Single Domain:** DGI (Veličković et al. 2019), GraphCL (You et al. 2020), GraphPrompt (Liu et al. 2023b).
- **Multi Domain:** MDGPT (Yu et al. 2024), GCOPE (Zhao et al. 2024), GraphBridge (Ju et al. 2025).
- **Robust GFM:** MDGFM (Wang et al. 2025).

Pre-training and Fine-tuning. We focus on **two** settings:

- **Cross-Datasets:** Pre-training and fine-tuning on **different** datasets from the **same** domain. While one dataset is selected as the target, the rest are sources.
- **Cross-Domain:** Pre-training and fine-tuning on **different** datasets from the **different** domain.

Few-shot Fine-tuning. We adopt a C -way 5-shot setting for each class. For graph classification, ego-graphs centered on target nodes are used, inheriting center label. Accuracy with standard deviation is used for evaluation over 20 runs.

Noise and Attack. We assess robustness in **two** scenarios:

- **Non-targeted Attack (Noise):** We inject random noise by perturbing either the structure or node features, with a perturbation rate $\lambda \in \{0.4, 0.8\}$. (1) For node feature attacks, we randomly inject Gaussian noise. (2) For structure attacks, we randomly remove edges from the graph.
- **Targeted Attack:** We employ the powerful NETTACK (Zügner, Akbarnejad, and Günnemann 2018) platform to perform attacks on specific nodes with the default number of perturbations $p \in \{1, 2, 3\}$. (1) For evasion attacks, the model is finetuned on a clean support set and attacked during testing on the query set. (2) For poisoning attacks, the entire support set is perturbed before fine-tuning.

Source	Cross-Dataset						Cross-Domain					
	Cora CiteSeer			Cora CiteSeer			Cora CiteSeer			ogbn-Home ogbn-Tech		
	ogbn-Home	Wiki-CS	PubMed	ogbn-Home	Wiki-CS	PubMed	ogbn-Home	Wiki-CS	ogbn-Home	Wiki-CS	ogbn-Home	Wiki-CS
Target	PubMed						ogbn-Home					
Noise & Attacks	feat.	struct.	evas.	pois.	feat.	struct.	evas.	pois.	feat.	struct.	evas.	pois.
GCN (backbone)	44.6 \pm 8.7	40.9 \pm 9.8	36.7 \pm 11.0	32.4 \pm 9.9	42.9 \pm 11.9	51.0 \pm 12.9	47.8 \pm 13.6	46.4 \pm 13.4	38.4 \pm 6.9	42.5 \pm 9.9	33.8 \pm 7.6	38.5 \pm 8.8
GAT	43.9 \pm 7.8	44.2 \pm 9.1	37.5 \pm 8.6	38.3 \pm 8.3	43.9 \pm 9.3	53.5 \pm 6.7	46.5 \pm 6.3	56.0 \pm 7.7	37.1 \pm 6.2	46.6 \pm 4.9	34.4 \pm 5.6	37.6 \pm 6.7
DGI	46.7 \pm 7.9	41.2 \pm 7.5	42.1 \pm 7.6	35.9 \pm 8.9	48.7 \pm 7.0	61.0 \pm 6.2	54.0 \pm 4.9	51.0 \pm 10.6	45.6 \pm 5.6	44.1 \pm 7.7	41.1 \pm 6.5	45.9 \pm 5.1
GraphCL	54.9 \pm 9.5	48.9 \pm 8.8	42.7 \pm 7.8	37.5 \pm 7.6	47.7 \pm 9.1	48.9 \pm 7.8	55.9 \pm 6.6	53.0 \pm 9.1	42.8 \pm 6.2	49.3 \pm 5.6	42.4 \pm 6.1	41.3 \pm 4.7
GraphPrompt	47.8 \pm 8.8	45.2 \pm 8.1	45.3 \pm 7.5	39.6 \pm 6.1	56.0 \pm 7.3	58.0 \pm 8.4	55.3 \pm 8.3	53.5 \pm 6.6	51.9 \pm 5.9	41.5 \pm 7.1	39.4 \pm 8.1	32.5 \pm 3.7
MDGPT	48.6 \pm 4.2	56.5 \pm 5.5	52.0 \pm 6.4	42.1 \pm 5.8	59.3 \pm 25.1	54.8 \pm 25.1	54.0 \pm 24.1	57.4 \pm 16.4	42.1 \pm 7.0	50.4 \pm 5.0	49.5 \pm 8.9	40.4 \pm 7.2
GCOPE	53.2 \pm 13.3	55.6 \pm 11.4	48.7 \pm 10.9	44.7 \pm 9.4	57.0 \pm 23.5	56.0 \pm 24.4	55.6 \pm 24.3	50.0 \pm 23.9	46.6 \pm 9.3	46.8 \pm 11.8	42.0 \pm 10.6	43.6 \pm 11.4
GraphBridge	51.1 \pm 6.8	52.4 \pm 4.3	44.0 \pm 10.1	46.9 \pm 7.4	63.0 \pm 4.5	62.2 \pm 5.2	57.1 \pm 3.7	51.3 \pm 6.6	50.1 \pm 6.6	47.3 \pm 5.7	43.2 \pm 10.1	42.4 \pm 8.3
MDGFM	57.3 \pm 6.7	58.4 \pm 7.3	53.4 \pm 7.3	50.8 \pm 5.2	65.0 \pm 15.9	65.3 \pm 17.0	62.9 \pm 15.3	62.1 \pm 16.2	53.2 \pm 6.9	52.0 \pm 5.2	50.1 \pm 6.2	46.4 \pm 5.7
SA²GFM (ours)	60.0\pm5.2	60.1\pm4.1	56.9\pm9.8	54.5\pm1.2	68.9\pm6.2	69.0\pm5.2	65.9\pm2.7	64.0\pm1.3	55.9\pm5.3	55.9\pm1.4	53.3\pm4.9	50.6\pm1.2

Table 1: Accuracy (%) \pm std. for 20 runs) of **5-shot node classification**. Best scores are in **bold**, runner-ups are underlined. “feat.” and “struct.” denote non-targeted attacks ($\lambda = 0.4$), while “evas.” and “pois.” denote targeted attacks ($p = 3$).

Source	Cross-Dataset						Cross-Domain					
	CiteSeer PubMed			Cora CiteSeer PubMed			Cora CiteSeer			ogbn-Home ogbn-Tech		
	CiteSeer	PubMed	ogbn-Home	CiteSeer	PubMed	ogbn-Home	CiteSeer	PubMed	ogbn-Home	ogbn-Tech	Wiki-CS	
Target	Cora						ogbn-Tech					
Noise & Attacks	feat.	struct.	evas.	pois.	feat.	struct.	evas.	pois.	feat.	struct.	evas.	pois.
GCN (backbone)	44.9 \pm 8.0	51.2 \pm 5.8	42.9 \pm 5.8	42.3 \pm 7.4	68.7 \pm 12.9	67.4 \pm 11.6	60.7 \pm 10.6	59.2 \pm 9.8	52.6 \pm 10.9	43.8 \pm 11.7	40.8 \pm 6.7	41.4 \pm 9.6
GAT	47.1 \pm 5.3	48.2 \pm 5.8	45.4 \pm 5.4	48.2 \pm 6.8	71.1 \pm 8.4	69.0 \pm 10.0	64.6 \pm 10.3	59.1 \pm 9.7	46.6 \pm 8.2	45.2 \pm 4.0	45.7 \pm 5.4	48.8 \pm 5.7
DGI	49.6 \pm 5.4	53.0 \pm 5.2	54.6 \pm 6.5	50.7 \pm 5.1	71.7 \pm 7.0	71.9 \pm 8.3	70.2 \pm 7.7	62.9 \pm 7.4	52.0 \pm 5.7	49.2 \pm 4.8	45.1 \pm 5.1	49.0 \pm 4.5
GraphCL	54.5 \pm 4.6	58.5 \pm 5.5	52.2 \pm 6.6	43.9 \pm 5.5	77.2 \pm 5.2	76.9 \pm 6.3	73.3 \pm 6.6	54.0 \pm 6.8	61.6 \pm 6.3	50.5 \pm 3.5	48.9 \pm 4.2	43.1 \pm 3.7
GraphPrompt	69.0 \pm 5.8	57.1 \pm 5.3	50.3 \pm 4.8	50.8 \pm 4.8	83.0 \pm 9.6	73.8 \pm 10.2	75.3 \pm 9.4	61.1 \pm 9.5	52.3 \pm 6.3	60.1 \pm 4.2	47.8 \pm 5.0	50.5 \pm 6.6
MDGPT	63.5 \pm 6.2	64.2 \pm 6.2	60.0 \pm 8.1	53.9 \pm 6.1	73.3 \pm 8.7	79.1 \pm 6.4	73.6 \pm 7.3	68.8 \pm 8.9	56.0 \pm 8.3	53.6 \pm 7.4	55.2 \pm 7.5	49.0 \pm 8.3
GCOPE	59.2 \pm 10.1	63.5 \pm 7.1	58.7 \pm 11.0	58.5 \pm 8.3	76.3 \pm 11.2	81.5 \pm 8.5	72.1 \pm 6.5	79.6 \pm 6.6	50.1 \pm 12.1	54.5 \pm 17.6	52.4 \pm 14.7	40.1 \pm 10.6
GraphBridge	62.4 \pm 5.0	61.0 \pm 4.8	62.1 \pm 5.7	56.6 \pm 5.0	81.0 \pm 7.5	80.8 \pm 10.6	76.9 \pm 7.7	73.9 \pm 7.0	61.5 \pm 3.6	56.5 \pm 3.6	58.6 \pm 3.6	48.6 \pm 3.6
MDGFM	65.9 \pm 4.7	67.8 \pm 4.9	65.8 \pm 6.3	62.6 \pm 5.8	85.3 \pm 9.7	85.9 \pm 7.6	83.1 \pm 8.8	83.5 \pm 9.6	66.4 \pm 5.2	62.9 \pm 4.6	61.5 \pm 6.7	56.5 \pm 8.0
SA²GFM (ours)	69.5\pm6.5	69.7\pm5.5	68.4\pm1.5	64.6\pm1.4	87.7\pm9.5	87.8\pm9.4	86.7\pm6.5	82.6\pm1.4	64.4\pm8.5	64.2\pm6.4	63.5\pm3.5	59.0\pm1.2

Table 2: Accuracy (%) \pm std. over 20 runs) of **5-shot graph classification**. Notations are consistent with Table 1.

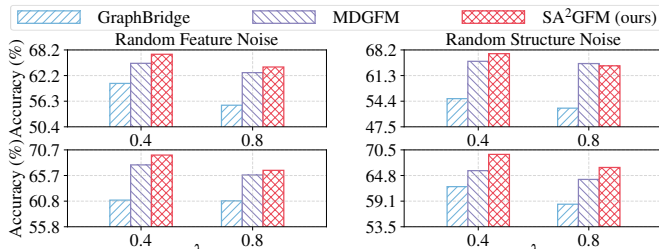


Figure 4: Performance on Cora with varying random noise perturbations (λ): node (top) and graph (bottom) classification.

5.2 RQ1: Against Noise and Adversarial Attacks

Results (Tables 1, Table 2) demonstrate that: ① Under both the node and graph classification, SA²GFM consistently outperforms all attacks. On average, it achieves +5.9% (node) and +2.4% (graph) accuracy improvements over the runner-up, indicating the strong robustness of SA²GFM to both non-targeted and target attacks. ② Compared to MDGFM, the strongest baseline with a robust domain adaptation module, SA²GFM achieves +5.1% average gain in the chal-

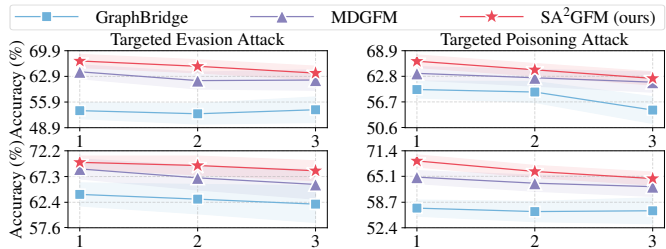


Figure 5: Performance on Cora with varying adversarial attack degree (p): node (top) and graph (bottom) classification.

lenging cross-domain settings, confirming its superiority in mitigating negative transfer under the large domain shifts. ③ Compared to other baselines without or weaker robustness designs, SA²GFM achieves an average improvement of +12.5%, verifying the impact of our structure-aware pre-training and null-expert routing, which together suppress spurious correlations and prevent negative transfer, contributing to more stable and robust adaptation under various perturbation scenarios. ④ Additional results in Appendix D.

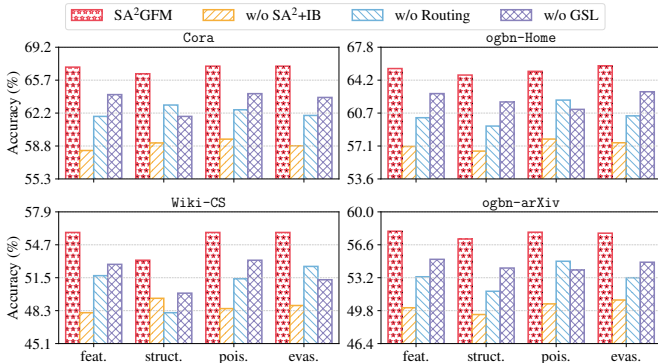


Figure 6: Ablation study on node classification under the non-targeted (random, $\lambda = 0.4$) and targeted ($p = 1$) attacks.

5.3 RQ2: Analysis of Perturbation Degree

We next systematically evaluate the performance degradation of under progressively intensified perturbations. Results (Figure 4 and Figure 5) show that: ① Though the performance of all methods degrades as the noise degree or attack severity increases, the drop of SA²GFM is significantly slower and more stable throughout. ② This observed trend suggests that SA²GFM not only achieves stronger base-level robustness but also maintains prediction stability under escalating perturbation levels. ③ Notably, in the most severe settings (*e.g.*, $\lambda = 0.8$ or $p = 3$), SA²GFM consistently outperforms the selected strong baselines MDGFM and Graph-Bridge by large margins in both node and graph classification, demonstrating its robustness and scalability.

5.4 RQ3: Ablation Study

We construct three variants to assess the key components.

- **SA²GFM (w/o SA² + IB):** removes both the Structure-Aware Semantic-Augmentation and the self-supervised IB module described in Section 4.1.
- **SA²GFM (w/o Routing):** removes the selective expert routing mechanism described in Section 4.2.
- **SA²GFM (w/o GSL):** removes the hierarchical structure optimization module described in Section 4.3.

Results (Figure 6) reveal all three components contribute to its robustness with varying impact. ① Removing “SA²+IB” causes the largest drop in accuracy, confirming its key role in learning the transferable, noise-resistant representations. ② Removing “Routing” degrades performance, especially under targeted attacks. ③ Removing “GSL” leads to reduced accuracy, particularly under structural perturbations. ④ Overall, the full SA²GFM achieves superior robustness through the coordinated contributions of each modules.

5.5 RQ4: Analysis of Hyperparameter Sensitivity

We analyze the sensitivity of SA²GFM to four key hyperparameters: τ , λ_{IB} , λ_m , and λ_u . Results (Figure 7) demonstrate that SA²GFM is generally stable across a wide range of hyperparameters. ① Each of the parameters exhibits a smooth performance curve, with optimal values around the default setting. ② Notably, $\lambda_{IB} = 10^{-2}$ and $\lambda_m = 0.5$ yield the highest robustness under targeted poisoning attacks, while overly

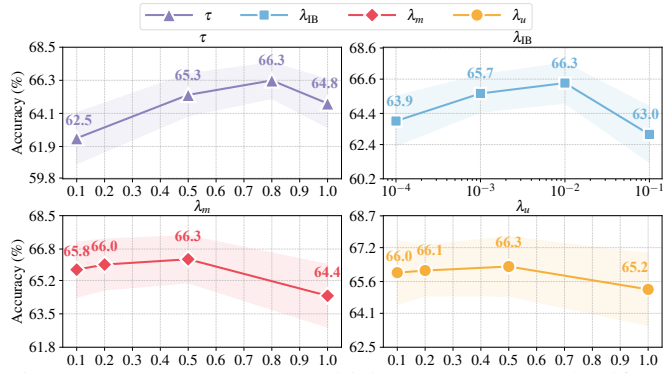


Figure 7: Hyperparameter sensitivity study on node classification under the targeted poisoning attack ($p = 1$).

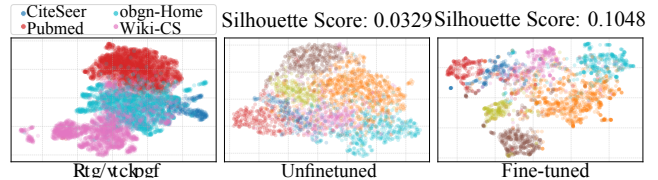


Figure 8: Node embeddings on Cora (cross-dataset).

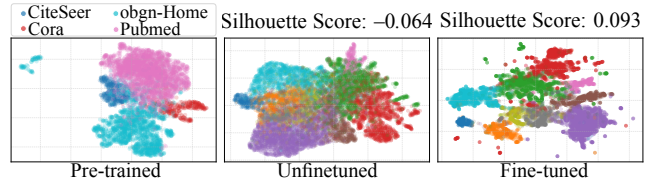


Figure 9: Node embeddings on Wiki-CS (cross-domain).

small or large values lead to moderate drops. ③ The trends suggest that while tuning improves robustness, the model is not overly sensitive to fluctuations, demonstrating reliable performance without extensive parameter searching.

5.6 RQ5: Embedding Visualizations

We utilize the UMAP (McInnes et al. 2018) to visualize the node embeddings and employ the Silhouette Score to evaluate the quality of class-wise clustering (the larger, the better). As shown in Figure 8 and Figure 9, the pre-trained embeddings have captured transferable structural and semantic patterns, evidenced by the domain-level separation. However, class-wise separability remains weak without fine-tuning. After fine-tuning, the embeddings become more clustered along class boundaries, with increased Silhouette Scores, confirming effective task-specific alignment.

6 Conclusion

In this work, we propose a robust graph foundation model SA²GFM. Through unified pre-training and fine-tuning, our method effectively bridges upstream transferable knowledge with downstream structural adaptation. Extensive experiments demonstrate that SA²GFM achieves superior robustness against both the random noise and adversarial perturbations, as well as strong generalization across domains, and consistently yields gains from its key modules, offering a promising foundation for reliable and adaptable GFM.

Acknowledgments

The corresponding author is Qingyun Sun. This work is supported in part by the National Natural Science Foundation of China (NSFC) under grants No. 62427808 and No. 623B2010, by the Fundamental Research Funds for the Central Universities, and by the Basic Ability Enhancement Program for Young and Middle-aged Teachers of Guangxi (No. 2024KY0073). We extend our sincere thanks to all authors for their valuable contributions.

References

Alemi, A. A.; Fischer, I.; Dillon, J. V.; and Murphy, K. 2017. Deep variational information bottleneck. In *ICLR*.

Bai, L.; Xu, Z.; Cui, L.; Li, M.; Wang, Y.; and Hancock, E. R. 2024. HC-GAE: The hierarchical cluster-based graph auto-encoder for graph representation learning. In *NeurIPS*.

Dan, J.; Liu, W.; Xie, C.; Yu, H.; Dong, S.; and Tan, Y. 2024. TFGDA: Exploring topology and feature alignment in semi-supervised graph domain adaptation through robust clustering. In *NeurIPS*, volume 37, 50230–50255.

Gasteiger, J.; Bojchevski, A.; and Günnemann, S. 2019. Combining neural networks with personalized pagerank for classification on graphs. In *ICLR*.

Giles, C. L.; Bollacker, K. D.; and Lawrence, S. 1998. CiteSeer: An automatic citation indexing system. In *Proceedings of the Third ACM Conference on Digital libraries*, 89–98.

Hu, W.; Fey, M.; Zitnik, M.; Dong, Y.; Ren, H.; Liu, B.; Catasta, M.; and Leskovec, J. 2020a. Open graph benchmark: Datasets for machine learning on graphs. In *NeurIPS*, volume 33, 22118–22133.

Hu, W.; Liu, B.; Gomes, J.; Zitnik, M.; Liang, P.; Pande, V.; and Leskovec, J. 2020b. Strategies for pre-training graph neural networks. In *ICLR*.

Huang, S.; Xu, Y.; Zhang, H.; and Li, X. 2025. Learn beneficial noise as graph augmentation. In *ICML*.

Ju, L.; Yang, X.; Li, Q.; and Wang, X. 2025. GraphBridge: Towards arbitrary transfer learning in GNNs. In *ICLR*.

Kataria, M.; Kumar, S.; and Jayadeva. 2024. UGC: Universal graph coarsening. In *NeurIPS*, 63057–63081.

Kipf, T. N.; and Welling, M. 2017. Semi-supervised classification with graph convolutional networks. In *ICLR*.

Lee, W.; and Park, H. 2025. Self-supervised adversarial purification for graph neural networks. In *ICML*.

Li, A.; and Pan, Y. 2016. Structural Information and Dynamical Complexity of Networks. *IEEE Transactions on Information Theory*, 62(6).

Li, H.; Wang, X.; Zhu, X.; Wen, W.; and Zhu, W. 2025. Disentangling invariant subgraph via variance contrastive estimation under distribution shifts. In *ICML*. Poster.

Liu, J.; Yang, C.; Lu, Z.; Chen, J.; Li, Y.; Zhang, M.; Bai, T.; Fang, Y.; Sun, L.; Yu, P. S.; et al. 2023a. Towards graph foundation models: A survey and beyond. *CoRR*.

Liu, Z.; Yu, X.; Fang, Y.; and Zhang, X. 2023b. Graph-Prompt: Unifying pre-training and downstream tasks for graph neural networks. In *WWW*, 417–428.

Long, Q.; Jin, Y.; Song, G.; Li, Y.; and Lin, W. 2020. Graph structural-topic neural network. In *KDD*, 1065–1073.

McCallum, A. K.; Nigam, K.; Rennie, J.; and Seymore, K. 2000. Automating the construction of internet portals with machine learning. *Information Retrieval*, 3: 127–163.

McInnes, L.; Healy, J.; Saul, N.; and Großberger, L. 2018. UMAP: Uniform manifold approximation and projection. *Journal of Open Source Software*, 3(29): 861.

Mernyei, P.; and Cangea, C. 2020. Wiki-CS: A Wikipedia-based benchmark for graph neural networks. *arXiv preprint arXiv:2007.02901*.

Morris, C.; Ritzert, M.; Fey, M.; Hamilton, W. L.; Lenssen, J. E.; Rattan, G.; and Grohe, M. 2019. Weisfeiler and leman go neural: Higher-order graph neural networks. In *AAAI*, volume 33, 4602–4609.

Oord, A. v. d.; Li, Y.; and Vinyals, O. 2018. Representation learning with contrastive predictive coding. *arXiv preprint arXiv:1807.03748*.

Poole, B.; Ozair, S.; Van Den Oord, A.; Alemi, A.; and Tucker, G. 2019. On variational bounds of mutual information. In *ICML*, 5171–5180. PMLR.

Sen, P.; Namata, G.; Bilgic, M.; Getoor, L.; Galligher, B.; and Eliassi-Rad, T. 2008. Collective classification in network data. *AI magazine*, 29(3): 93–93.

Stewart, G. W. 1993. On the early history of the singular value decomposition. *SIAM Review*, 35(4): 551–566.

Tang, J.; Yang, Y.; Wei, W.; Shi, L.; Xia, L.; Yin, D.; and Huang, C. 2024. HiGPT: Heterogeneous Graph Language Model. In *KDD*, 2842–2853.

Tishby, N.; Pereira, F. C.; and Bialek, W. 1999. The information bottleneck method. In *Proceedings of the 37th Annual Allerton Conference on Communication, Control and Computing*, 368–377.

Veličković, P.; Cucurull, G.; Casanova, A.; Romero, A.; Liò, P.; and Bengio, Y. 2018. Graph attention networks. In *ICLR*.

Veličković, P.; Fedus, W.; Hamilton, W. L.; Liò, P.; Bengio, Y.; and Hjelm, R. D. 2019. Deep graph infomax. In *ICLR*.

Wang, Q.; Wang, Y.; Wang, Y.; and Ying, X. 2024. Dissecting the failure of invariant learning on graphs. In *NeurIPS*.

Wang, S.; Wang, B.; Shen, Z.; Deng, B.; and Kang, Z. 2025. Multi-domain graph foundation models: Robust knowledge transfer via topology alignment. In *ICML*.

Xu, K.; Hu, W.; Leskovec, J.; and Jegelka, S. 2019. How powerful are graph neural networks? In *ICLR*.

You, Y.; Chen, T.; Sui, Y.; Chen, T.; Wang, Z.; and Shen, Y. 2020. Graph contrastive learning with augmentations. In *NeurIPS*, 1–12.

Yu, X.; Zhou, C.; Fang, Y.; and Zhang, X. 2024. Text-free multi-domain graph pre-training: Toward graph foundation models. *arXiv preprint arXiv:2405.13934*.

Yuan, H.; Sun, Q.; Fu, X.; Ji, C.; and Li, J. 2024. Dynamic Graph Information Bottleneck. In *WWW*, 469–480.

Yuan, H.; Sun, Q.; Fu, X.; Zhang, Z.; Ji, C.; Peng, H.; and Li, J. 2023. Environment-aware dynamic graph learning for out-of-distribution generalization. *NeurIPS*, 36.

Yuan, H.; Sun, Q.; Shi, J.; Fu, X.; Hooi, B.; Li, J.; and Yu, P. S. 2025a. GRAVER: Generative Graph Vocabularies for Robust Graph Foundation Models Fine-tuning. In *NeurIPS*.

Yuan, H.; Sun, Q.; Shi, J.; Fu, X.; Hooi, B.; Li, J.; and Yu, P. S. 2025b. How much can transfer? BRIDGE: Bounded multi-domain graph foundation model with generalization guarantees. In *ICML*.

Yuan, H.; Sun, Q.; Wang, Z.; Fu, X.; Ji, C.; Wang, Y.; Jin, B.; and Li, J. 2025c. DG-Mamba: Robust and efficient dynamic graph structure learning with selective state space models. In *AAAI*, volume 39, 22272–22280.

Zhang, G.; Dong, H.; Zhang, Y.; Li, Z.; Chen, D.; Wang, K.; Chen, T.; Liang, Y.; Cheng, D.; and Wang, K. 2024. GDeR: Safeguarding efficiency, balancing, and Robustness via Prototypical Graph Pruning. In *NeurIPS*.

Zhao, H.; Chen, A.; Sun, X.; Cheng, H.; and Li, J. 2024. All in one and one for all: A simple yet effective method towards cross-domain graph pretraining. In *KDD*, 4443–4454.

Zheng, S.; Wang, H.; and Liu, X. 2024. IntraMix: Intra-class mixup generation for accurate labels and neighbors. In *NeurIPS*, 8951–8980.

Zhu, Y.; Xu, W.; Zhang, J.; Liu, Q.; Wu, S.; and Wang, L. 2021. Deep graph structure learning for robust representations: A survey. *arXiv preprint arXiv:2103.03036*, 14: 1–1.

Zügner, D.; Akbarnejad, A.; and Günnemann, S. 2018. Adversarial attacks on neural networks for graph data. In *KDD*, 2847–2856.

A Algorithms and Complexity Analysis

SA²GFM includes two stages: pre-training and fine-tuning. We illustrate the pipeline for each stage in Algorithm 1 and Algorithm 2. The complexity is analyzed as follows.

Algorithm 1: The pre-training pipeline of SA²GFM.

Input: Source graphs $\{G_i^S = (\mathbf{A}_i^S, \mathbf{X}_i^S)\}_{i=1}^n$; Pre-training epochs E_p ; Learning rate η_p ; Hyperparameter λ_{IB} .
Output: Pre-trained encoders $\{\mathcal{F}_{\Theta_i}^*\}_{i=1}^n$.

```

1: for each  $G_i^S$  in  $\{G_i^S\}_{i=1}^n$  do
2:   Partition  $G_i^S$  into  $K$  clusters using structural entropy;
3:   for each node  $v_j$  in  $G_i^S$  do
4:     Generate text  $t_j$  for  $v_j$  based on cluster context;
5:     Compute augmented feature:  $\mathbf{x}_j^{S'} \leftarrow$  Eq. (1);
6:   end for
7:   Obtain the augmented feature matrix  $\mathbf{X}_i^{S'}$ ;
8:   Initialize encoder parameters  $\Theta_i$ ;
9:   for epoch  $e = 1, \dots, E_p$  do
10:    Sample a batch of positive and negative pairs;
11:     $(\mu_i, \sigma_i) \leftarrow \mathcal{F}_{\Theta_i}(\mathbf{A}_i^S, \mathbf{X}_i^{S'})$ ;
12:     $\mathbf{Z}_i^S \leftarrow \mu_i + \epsilon \odot \sigma_i$ ,  $\epsilon \sim \mathcal{N}(0, \mathbf{I})$ ;
13:    Compute contrastive loss:  $\mathcal{L}_{InfoNCE} \leftarrow$  Eq. (4);
14:    Compute compression loss:  $\mathcal{L}_{KL} \leftarrow$  Eq. (5);
15:    Compute total loss:  $\mathcal{L}_{pretrain} \leftarrow$  Eq. (7);
16:    Update  $\Theta_i$  by back-propagation.
17:  end for
18: end for

```

A.1 Computational Complexity Analysis of the Pre-training Stage (Algorithm 1)

This section aims to provide a detailed breakdown of the computational complexity of the SA²GFM during the multi-domain pre-training stage, as outlined in Algorithm 1. The overall cost of the pre-training stage is primarily composed of two parts: a one-time Structure-Aware Semantic Augmentation for each source graph, followed by the iterative Self-Supervised Information Bottleneck training.

We analyze the computational cost for a single iteration of the outer loop in the algorithm (Line 1), which processes a single source graph $G_i^S = (\mathbf{A}_i^S, \mathbf{X}_i^S)$. This graph contains $|\mathcal{V}_i|$ nodes and $|\mathcal{E}_i|$ edges.

Structure-Aware Semantic Augmentation (Lines 2-7). This step generates the augmented node feature matrix $\mathbf{X}_i^{S'}$ for each source graph and is a pre-processing procedure.

- **Structural Entropy Partitioning (Line 2):** Computing the optimal hierarchical partition (encoding tree) for the graph G_i^S has a complexity of $\mathcal{O}(|\mathcal{E}_i| \log |\mathcal{V}_i|)$.
- **Feature Augmentation (Lines 3-6):** The algorithm generates a text prompt t_j and computes the augmented feature $\mathbf{x}_j^{S'}$ for each node v_j in the graph. This process involves using BERT and SVD. The total complexity for performing this operation on all $|\mathcal{V}_i|$ nodes is approximately $\mathcal{O}(|\mathcal{V}_i| \cdot (C_{BERT} + (d_i + d_{BERT}) \cdot d_0))$, where C_{BERT} represents the BERT inference cost, d_i and d_{BERT} are the dimensions of the original features and BERT embeddings respectively, and d_0 is the aligned dimension.

The cost of this step is amortized over the entire training process and is typically much smaller than the subsequent iterative training cost.

Self-Supervised Information Bottleneck (SS-IB) Training (Lines 8-16). SS-IB is the computational core of the pre-training, where it trains an expert encoder \mathcal{F}_{Θ_i} independently for each source graph G_i^S over E_p epochs.

- **Encoder Forward Pass (Line 11):** In each epoch, the main computation is the forward pass of the GNN encoder \mathcal{F}_{Θ_i} . It takes the adjacency matrix \mathbf{A}_i^S and the augmented feature matrix $\mathbf{X}_i^{S'}$ as input. For an L -layer GNN, a single forward pass on a sparse graph has a complexity of $\mathcal{O}(L \cdot |\mathcal{E}_i| \cdot d)$, where d is the hidden feature dimension.
- **Loss Computation and Backpropagation (Lines 13-16):** The complexity of computing $\mathcal{L}_{InfoNCE}$ and \mathcal{L}_{KL} is linear with respect to the number of nodes $|\mathcal{V}_i|$, i.e., $\mathcal{O}(|\mathcal{V}_i| \cdot d)$. The update of parameters Θ_i depends on the back-propagation through the entire computation graph, which has a complexity comparable to the forward pass. Therefore, the main cost of a single iteration is dominated by the GNN computation.
- **Total Training Cost:** Repeating this process for E_p epochs, the total complexity for training a single expert encoder \mathcal{F}_{Θ_i} is $\mathcal{O}(E_p \cdot L \cdot |\mathcal{E}_i| \cdot d)$.

Overall Pre-training Complexity. The outer loop of Algorithm 1 (Line 1) indicates that the above process is performed independently for all n source domains. Therefore, the total computational complexity of pre-training is the sum of the training costs for all n experts. The final complexity is determined by the number of pre-training epochs (E_p), the number of layers in the GNN encoder (L), and its hidden feature dimension (d). Assuming an average number of edges $|\mathcal{E}|$ across all graphs, the overall complexity is:

$$\mathcal{O}(n \cdot E_p \cdot L \cdot |\mathcal{E}| \cdot d) \quad (\text{A.1})$$

The analysis shows the pre-training complexity scales linearly with the number of source domains and the number of edges in the graphs, enabling it to efficiently scale to multi-domain and large-scale graph scenarios.

A.2 Computational Complexity Analysis of the Fine-tuning Stage (Algorithm 2)

The fine-tuning stage, outlined in Algorithm 2, adapts the pre-trained model to a target graph $G^T = (\mathbf{A}^T, \mathbf{X}^T)$ with $|\mathcal{V}_T|$ nodes and $|\mathcal{E}_T|$ edges, where the number of fine-tuning epochs, E_f , is small. The complexity analysis is broken down into a one-time preprocessing step and the per-epoch iterative training cost.

Preprocessing (Lines 1-6). Before the main training loop, the model performs a series of one-time setup operations.

- **Parameter Initialization (Line 1):** This involves initializing the learnable parameters, including the routing network \mathcal{R}_ϕ and the prompts \mathcal{P}_Ω . The calculation of initial routing weights α requires computing prototypes from the small, few-shot support set, making its cost negligible.

Algorithm 2: The fine-tuning pipeline of SA²GFM.

Input: 5 nodes class-balanced sampled from a target graphs $\{G^T\} \in \mathcal{G}^T$ (node classification) or 5 target graphs $\{G^T\} \in \mathcal{G}^T$ from target domain $\{D^T\} \in \mathcal{D}^T$ (graph classification); Pre-trained experts $\{\mathcal{F}_{\Theta_i}^*\}_{i=1}^n$; Epochs E_f ; Expert routing network \mathcal{R}_ϕ ; Learnable prompt \mathcal{P}_Ω ; Learning rate η_f ; Hyperparameters λ_m, λ_u .

Output: Fine-tuned SA²GFM with $\{\Theta^*, \phi^*, \Omega^*\}$.

- 1: Initialize the routing network: $\alpha \leftarrow$ Eq. (8) and Eq. (9); and randomly initialize other parameters Ω ;
- 2: Partition G^T into clusters \mathcal{C}^T using structural entropy;
- 3: **for** each node v_i in G^T **do**
- 4: Compute augmented feature: $\mathbf{x}_i^T \leftarrow$ Eq. (1);
- 5: **end for**
- 6: Obtain augmented feature matrix \mathbf{X}^T ;
- 7: **for** $e = 1, \dots, E_f$ **do**
- 8: Compute MoE regularization loss: $\mathcal{L}_{\text{MoE}} \leftarrow$ Eq. (12);
- 9: Compute uncertainty loss: $\mathcal{L}_{\text{uncertain}} \leftarrow$ Eq. (14);
- 10: Refine target graph structure: $\mathbf{A}^T \leftarrow$ Eq. (17);
- 11: Generate final embeddings: $\mathbf{Z}^T \leftarrow$ Eq. (18);
- 12: Compute classification loss: $\mathcal{L}_{\text{cls}} \leftarrow$ Eq. (19);
- 13: Compute fine-tuning loss: $\mathcal{L}_{\text{finetune}} \leftarrow$ Eq. (20);
- 14: Update $\{\phi, \Omega\}$ by back-propagation.
- 15: **end for**

• **Structure-Aware Semantic Augmentation (Lines 2-6):**

The calculation process for this step is identical to that of the pre-training stage and is performed only once. It consists of two main parts: Structural Entropy Partitioning (Line 2) with a complexity of $\mathcal{O}(|\mathcal{E}_T| \log |\mathcal{V}_T|)$, and Feature Augmentation (Lines 3-6) with a complexity of $\mathcal{O}(|\mathcal{V}_T| \cdot (C_{\text{BERT}} + (d_i + d_{\text{BERT}}) \cdot d_0))$.

Per-Epoch Training Complexity (Lines 7-14). The main computational load resides within the fine-tuning loop, which runs for E_f epochs.

• **Loss Computations for Regularization (Lines 8-9):** The calculation of the MoE loss \mathcal{L}_{MoE} and the uncertainty loss $\mathcal{L}_{\text{uncertain}}$ are computationally inexpensive. \mathcal{L}_{MoE} is an entropy calculation over $n + 1$ weights, costing $\mathcal{O}(n)$. The cost of $\mathcal{L}_{\text{uncertain}}$ is tied to the attention score computation within the structure optimization step.

• **Hierarchical Structure Optimization (Line 10):** This is a significant part of the per-epoch computation. It refines the graph topology \mathbf{A}^T into $\mathbf{A}^{T'}$ by combining two components. First, *intra-cluster learning* uses multi-head attention within each cluster c , which has a complexity quadratic to cluster size, totaling $\mathcal{O}(\sum_{c \in \mathcal{C}^T} |\mathcal{V}_c|^2 \cdot d_k)$, where $|\mathcal{V}_c|$ is the number of nodes in cluster c . Secondly, *inter-cluster learning* uses an APPNP-like propagation for T steps, with a complexity of $\mathcal{O}(T \cdot |\mathcal{E}_T|)$.

• **Final Embedding Generation and Classification (Lines 11-12):** To compute the final classification loss \mathcal{L}_{cls} , the model first generates node embeddings \mathbf{Z}^T using the frozen pre-trained encoders $\{\mathcal{F}_{\Theta_i}^*\}_{i=1}^n$. This involves a full forward pass on the newly refined graph structure $\mathbf{A}^{T'}$. The complexity of this step is $\mathcal{O}(n \cdot L \cdot |\mathcal{E}_T'| \cdot d)$,

where $|\mathcal{E}_T'|$ is the number of edges in the optimized graph, which we can approximate as $\mathcal{O}(n \cdot L \cdot |\mathcal{E}_T| \cdot d)$.

Overall Fine-tuning Complexity. The one-time preprocessing costs are amortized and considered low-order terms. The dominant cost is within the training loop. Summing the complexities of the most expensive steps per epoch, the overall complexity for the fine-tuning stage is:

$$\mathcal{O}\left(E_f \cdot \left(\sum_c |\mathcal{V}_c|^2 d_k + T|\mathcal{E}_T| + nL|\mathcal{E}_T|d\right)\right) \quad (\text{A.2})$$

This formulation highlights that the per-epoch cost is independent of the number of experts n . The primary computational burden comes from the intra-cluster attention, making the process highly efficient for graphs that can be partitioned into reasonably small, balanced clusters. This efficiency is critical for the model’s applicability in few-shot learning contexts.

B Proofs

This section proves the approximation error bound of our practical objective with respect to the theoretical Self-Supervised Information Bottleneck (SS-IB) objective.

B.1 Proof of Derivation 1

We first restate Derivation 1 for reference.

Derivation 1 (Lower Bound of $I(\mathbf{Z}^S; \mathbf{Z}^{S+})$). Prediction term $I(\mathbf{Z}^S; \mathbf{Z}^{S+})$ is lower-bounded by InfoNCE (Oord, Li, and Vinyals 2018). For each anchor v_i and positive node v_i^+ :

$$I(\mathbf{Z}^S; \mathbf{Z}^{S+}) \geq -\mathcal{L}_{\text{InfoNCE}} = \frac{1}{N^+} \sum_{i=1}^{N^+} \log \frac{\exp(\langle \mathbf{Z}_i^S, \mathbf{Z}_i^{S+} \rangle / \tau)}{\sum_{j=0}^{N^-} \exp(\langle \mathbf{Z}_i^S, \mathbf{Z}_j^S \rangle / \tau)},$$

where N^+ and N^- are the number of positive and negative samples, which are non-redundantly and consistently sampled from the source domain depending on whether there is a direct link (Liu et al. 2023b). τ is a temperature.

Proof. We consider the standard mutual information:

$$I(\mathbf{Z}^S; \mathbf{Z}^{S+}) = \mathbb{E}_{p(\mathbf{Z}^S, \mathbf{Z}^{S+})} \left[\log \frac{p(\mathbf{Z}^S, \mathbf{Z}^{S+})}{p(\mathbf{Z}^S)p(\mathbf{Z}^{S+})} \right]. \quad (\text{B.1})$$

However, $p(\mathbf{Z}^S)$ and $p(\mathbf{Z}^{S+})$ is intractable. Following Oord, Li, and Vinyals (2018); Poole et al. (2019), we approximate by a classification-based surrogate using Noise-Contrastive Estimation (NCE), where it distinguishes N^+ positive samples \mathbf{Z}_i^{S+} from N^- negative samples $\{\mathbf{Z}_j^S\}_{j=0}^{N^-}$. Let $q(i|\mathbf{Z}^S)$ be the probability of correctly identifying the positive sample among a set of $(N^- + 1)$ candidates, defined as:

$$q(i^+|\mathbf{Z}^S) = \frac{\exp(\text{sim}(\mathbf{Z}^S, \mathbf{Z}_i^{S+}) / \tau)}{\sum_{j=0}^{N^-} \exp(\text{sim}(\mathbf{Z}^S, \mathbf{Z}_j^S) / \tau)}. \quad (\text{B.2})$$

Then, InfoNCE loss is given as the negative log-likelihood of identifying the positive:

$$\mathcal{L}_{\text{InfoNCE}} = -\mathbb{E}_p [\log q(i^+ | \mathbf{Z}^S)]. \quad (\text{B.3})$$

According to Theorem 1 from Poole et al. (2019), the mutual information can be lower-bounded as:

$$I(\mathbf{Z}^S; \mathbf{Z}^{S+}) \geq -\mathcal{L}_{\text{InfoNCE}}. \quad (\text{B.4})$$

This bound becomes tighter as N^- increases. In practice, N^- is the number of negative samples used per anchor. Let $\text{sim}(\mathbf{Z}_i^S, \mathbf{Z}_j^S) = \langle \mathbf{Z}_i^S, \mathbf{Z}_j^S \rangle$ denote dot-product similarity, the explicit form becomes:

$$\mathcal{L}_{\text{InfoNCE}} = \log \left(\sum_{j=0}^{N^-} \exp \frac{\langle \mathbf{Z}_i^S, \mathbf{Z}_j^S \rangle}{\tau} \right) - \frac{\langle \mathbf{Z}_i^S, \mathbf{Z}_i^{S+} \rangle}{\tau}. \quad (\text{B.5})$$

Thus, combining the above gives the desired lower bound:

$$I(\mathbf{Z}^S; \mathbf{Z}^{S+}) \geq -\mathcal{L}_{\text{InfoNCE}}. \quad (\text{B.6})$$

This concludes the proof. \square

B.2 Proof of Derivation 2

We first restate Derivation 2 for reference.

Derivation 2 (Upper Bound of $I(\mathbf{Z}^S; \mathbf{X}^{S'})$). Compression term $I(\mathbf{Z}^S; \mathbf{X}^{S'})$ is upper-bounded by the KL divergence between posterior $q(\mathbf{Z}^S | \mathbf{X}^{S'})$ and prior $p(\mathbf{Z}^S)$:

$$I(\mathbf{Z}^S; \mathbf{X}^{S'}) \leq \frac{1}{N} \sum_{i=1}^N \text{KL}[q(\mathbf{Z}_i^S | \mathbf{X}_i^{S'}) \parallel p(\mathbf{Z}_i^S)],$$

We assume a standard Gaussian prior $p(\mathbf{Z}^S) = \mathcal{N}(\mathbf{0}, \mathbf{I})$, and apply the graph encoder to produce the mean $\boldsymbol{\mu}_i$ and the log-variance $\log \boldsymbol{\sigma}_i^2$ of $q(\mathbf{Z}_i^S | \mathbf{X}_i^{S'})$ for each node v_i , from which we sample \mathbf{Z}_i^S via reparameterization trick:

$$\mathbf{Z}_i^S \sim q(\mathbf{Z}_i^S | \mathbf{X}_j^{S'}) = \mathcal{N}(\boldsymbol{\mu}_i, \text{diag}(\boldsymbol{\sigma}_i^2)).$$

Proof. The mutual information between the representation \mathbf{Z}^S and input $\mathbf{X}^{S'}$ is given by:

$$I(\mathbf{Z}^S; \mathbf{X}^{S'}) = \mathbb{E}_{p(\mathbf{X}^{S'})} [\text{KL}(q(\mathbf{Z}^S | \mathbf{X}^{S'}) \parallel q(\mathbf{Z}^S))]. \quad (\text{B.7})$$

However, the marginal distribution $q(\mathbf{Z}^S)$ is generally intractable. To obtain a tractable upper bound, we follow the Deep Variational Information Bottleneck (VIB) (Alemi et al. 2017), which replaces the intractable marginal $q(\mathbf{Z}^S)$ with a simple prior $p(\mathbf{Z}^S)$, yielding:

$$I(\mathbf{Z}^S; \mathbf{X}^{S'}) \leq \mathbb{E}_{p(\mathbf{X}^{S'})} [\text{KL}(q(\mathbf{Z}^S | \mathbf{X}^{S'}) \parallel p(\mathbf{Z}^S))]. \quad (\text{B.8})$$

Assume that the posterior $q(\mathbf{Z}_i^S | \mathbf{X}_i^{S'})$ is modeled as a multivariate Gaussian with diagonal covariance:

$$q(\mathbf{Z}_i^S | \mathbf{X}_i^{S'}) = \mathcal{N}(\boldsymbol{\mu}_i, \text{diag}(\boldsymbol{\sigma}_i^2)), \quad p(\mathbf{Z}_i^S) = \mathcal{N}(\mathbf{0}, \mathbf{I}). \quad (\text{B.9})$$

Then, the KL divergence for each node v_i becomes:

$$\begin{aligned} & \text{KL} [q(\mathbf{Z}_i^S | \mathbf{X}_i^{S'}) \parallel p(\mathbf{Z}_i^S)] \\ &= \frac{1}{2} \sum_{k=1}^d (\boldsymbol{\sigma}_{i,k}^2 + \boldsymbol{\mu}_{i,k}^2 - 1 - \log \boldsymbol{\sigma}_{i,k}^2). \end{aligned} \quad (\text{B.10})$$

Thus, the compression term is upper-bounded by the mean KL divergence across all nodes:

$$I(\mathbf{Z}^S; \mathbf{X}^{S'}) \leq \frac{1}{N} \sum_{i=1}^N \text{KL} [q(\mathbf{Z}_i^S | \mathbf{X}_i^{S'}) \parallel p(\mathbf{Z}_i^S)]. \quad (\text{B.11})$$

This bound is tight when the posterior matches the prior and serves as the regularization term in our SS-IB loss. This concludes the proof. \square

C Experiment Settings

In this section, we present experiment details of SA²GFM*. Dataset statistics are summarized in Table C.1.

C.1 Datasets

To evaluate multi-domain capabilities, we select **seven** graph datasets across **three** distinct domains in contrast to conventional settings where each dataset is treated as an independent domain. These datasets vary in structure, scale, and feature distribution, providing a diverse and challenging testbed for evaluating pre-trained graph models. A detailed statistical summary of these datasets is presented in Table C.1.

Citation Domain. This domain includes **four** widely used citation networks. Each dataset consists of a single graph, where nodes denote academic papers, edges denote citation relationships, and node labels correspond to the category or research topic of each paper.

- **Cora** (McCallum et al. 2000): A well-known citation network consisting of 2,708 machine learning papers divided into seven categories (e.g., Neural Networks, Reinforcement Learning). The graph contains 5,429 citation links. Each paper is represented by a 1,433-dimensional binary bag-of-words vector, indicating the presence or absence of words from a predefined dictionary.
- **CiteSeer** (Giles, Bollacker, and Lawrence 1998): Includes 3,186 scientific publications across six fields. It features 4,277 citation links. Similar to **Cora**, each publication is described by a 3,703-dimensional sparse binary vector representing its vocabulary.
- **PubMed** (Sen et al. 2008): A larger biomedical citation network derived from the PubMed database. It contains 19,717 research articles related to diabetes, classified into three categories. Each article is embedded by a 500-dimensional feature vector based on TF-IDF.
- **ogbn-arXiv** (Hu et al. 2020a): A large-scale citation graph, representing citations among 169,343 Computer Science papers from arXiv. The task is to predict the paper’s subject area from 40 categories. Node features are 128-dimensional vectors derived from the average embeddings of words in the title and abstract.

Products Domain. This domain includes **two** large-scale networks from OGB (Hu et al. 2020a), capturing relationships between products frequently co-purchased on Amazon. Nodes represent products with a 100-dimensional vector, and an edge indicates a co-purchase relationship, making them useful for recommendation-related tasks.

*<https://anonymous.4open.science/r/SA2GFM>.

Dataset	Domain	# Nodes	# Edges	# Feature Dimensions	# Classes	Avg. # Deg.
Cora (McCallum et al. 2000)	Citation	2,708	5,429	1,433	7	4.00
CiteSeer (Giles, Bollacker, and Lawrence 1998)	Citation	3,186	4,277	3,703	6	2.57
PubMed (Sen et al. 2008)	Citation	19,717	44,338	500	3	4.50
ogbn-arXiv (Hu et al. 2020a)	Citation	169,343	1,166,243	128	40	13.77
ogbn-Tech (Hu et al. 2020a)	Products	47,428	2,077,241	100	3	87.60
ogbn-Home (Hu et al. 2020a)	Products	9,790	131,841	100	5	26.93
Wiki-CS (Mernyei and Cangea 2020)	Web Page	11,701	216,123	300	10	36.94

Table C.1: Statistics of the benchmark graph datasets.

Type	Target Dataset	Source Datasets
Cross-Dataset	Cora	CiteSeer, PubMed, ogbn-Home, Wiki-CS
	CiteSeer	Cora, PubMed, ogbn-Home, Wiki-CS
	PubMed	Cora, CiteSeer, ogbn-Home, Wiki-CS
	ogbn-Tech	Cora, CiteSeer, PubMed, ogbn-Home, Wiki-CS
Cross-Domain	ogbn-Home	Cora, CiteSeer, PubMed, Wiki-CS
	Wiki-CS	Cora, CiteSeer, PubMed, ogbn-Home
	ogbn-arXiv	ogbn-Home, ogbn-Tech, Wiki-CS

Table C.2: Configuration of the pre-training source datasets for each target dataset.

- ogbn-Tech (Hu et al. 2020a): A technology products network, featuring 47,428 nodes and 3 product categories.
- ogbn-Home (Hu et al. 2020a): A home goods-related products network, consisting of 9,790 nodes and 5 product categories.

Web Page Domain. This domain features a graph constructed from web pages and their hyperlinks.

- Wiki-CS (Mernyei and Cangea 2020): A graph based on 11,701 Wikipedia articles on computer science topics, connected by 216,123 hyperlinks. Nodes are categorized into 10 areas. This dataset is specifically designed for robust evaluation with multiple data splits to prevent overfitting to a particular training set.

C.2 Baselines

We benchmark SA²GFM against nine state-of-the-art methods spanning **four** major categories.

Classic GNNs. Includes vanilla GCN (Kipf and Welling 2017) and GAT (Veličković et al. 2018) trained from scratch on downstream tasks without any pre-training. These models serve as fundamental baselines for evaluating representation learning performance.

Single-Domain Graph Pre-training. This category includes baselines that learn transferable representations by optimizing auxiliary tasks without annotations.

- GraphPrompt (Liu et al. 2023b): Introduces a prompt-based learning paradigm for graph pre-training to improve sample efficiency. It designs task-specific prompts to guide the model, enabling effective adaptation to downstream tasks with minimal fine-tuning.

- GraphCL (You et al. 2020): A general framework for learning node and graph representations through contrastive learning. It applies various data augmentations to the input graph and aims to maximize the agreement between representations of different augmented views.
- DGI (Veličković et al. 2019): An unsupervised approach for learning node representations by maximizing the mutual information between local patch representations and corresponding global graph summaries, achieved by contrasting the real graph with corrupted versions.

Multi-Domain Graph Pre-training. These methods aim to learn representations that generalize across heterogeneous domains by exploiting shared patterns.

- MDGPT (Yu et al. 2024): A text-free framework that aligns domains through learnable domain tokens.
- GraphBridge (Ju et al. 2025): A multi-domain graph pre-training and prompt learning framework that minimizes generalization error bounds. It introduces domain-invariant aligners and a lightweight MoE router for selective knowledge transfer.
- GCOPE (Zhao et al. 2024): A framework that enhances graph prompting through knowledgeable contextualization and prompt ensembling. It combines structural and semantic information in prompts and uses ensembles to improve robustness in few-shot settings.

Robust GFMs. The most related methods focus on enhancing the robustness of multi-domain pre-trained GFMs.

- MDGFM (Wang et al. 2025): A unified framework for robust multi-domain knowledge transfer that aligns graph topologies and eliminates noise via graph structure learning. It leverages domain tokens, balance tokens, and dual-prompt to ensure feature and topology alignment.

C.3 Experimental Setting Details

We introduce the detailed experimental settings.

Settings for Section 5.2 and 5.3 (RQ1, RQ2). This section evaluates the effectiveness and robustness of SA²GFM under the few-shot setting, using a (C -way) 5-shot configuration with 5 labeled samples per class.

Cross-Dataset and Cross-Domain Settings. We set two types of domain adaptation scenarios, with the detailed configurations shown in Table C.2. (1) For cross-dataset transfer, the target dataset is **unseen** during pre-training but comes from the **same** domain as the source datasets. (2) For cross-domain transfer, the target dataset originates from a **different** domain altogether. It is worth noting that, while some prior works on cross-domain graph pre-training and fine-tuning (Zhao et al. 2024; Yu et al. 2024) treat each dataset as a separate domain, we argue that such treatment is overly coarse. Instead, we define domains based on broader semantic or application categories. As a result, our cross-dataset setting corresponds to what previous literature often calls cross-domain, whereas our cross-domain setting reflects a higher-level shift across distinct fields.

5-shot Fine-tuning Settings. We randomly sample 5 labeled instances (nodes or graphs) per class to construct the support set, with the remaining labeled samples as the query set. To ensure stable evaluation and reduce sampling bias, we conduct 20 runs with different seeds and report the mean accuracy and standard deviation. We evaluate SA²GFM on both node and graph classification tasks. For graph classification, we build input graphs by extracting ego-graphs centered at target nodes.

Robustness against Non-targeted Attack Settings. To evaluate the robustness of SA²GFM under non-targeted perturbations (random noise) during fine-tuning, we introduce random noise to the support set from two complementary aspects: feature and structure. (1) For feature noise, we inject Gaussian perturbations into each feature dimension of the support samples, defined as $\lambda \cdot r \cdot \epsilon$, where r denotes the reference amplitude of the original features, $\epsilon \sim \mathcal{N}(0, 1)$ represents standard Gaussian noise, and $\lambda \in \{0.4, 0.8\}$ controls the noise level. (2) For structure noise, we randomly alter the support graph topology by randomly deleting a proportion λ of the edges. These controlled non-targeted attacks allow us to systematically assess the robustness of SA²GFM in few-shot adaptation scenarios.

Robustness against Targeted Attack Settings. To further assess the adversarial robustness of SA²GFM, we adopt NETTACK (Zügner, Akbarnejad, and Günnemann 2018), a widely applied targeted attack framework for graph data that perturbs either node features or edges of selected target nodes. We evaluate two standard attack modes: (1) Evasive attack, where the model is trained on clean support sets and adversarial perturbations are applied only during inference on the query set. (2) Poisoning attack, where perturbations are introduced into the support set before training. In both settings, we follow NETTACK’s default strategy to select vulnerable nodes and use GAT (Veličković et al. 2018) as the surrogate model with default parameters. The number of allowed perturbations is set as $n \in \{1, 2, 3\}$.

Detailed Settings for Section 5.4 (RQ3). To ensure a fair comparison, the ablation study is conducted on four representative datasets: Cora, ogbn-Home, Wiki-CS, and ogbn-arXiv, focusing on the 5-shot node classification task. To clearly observe each component’s contribution, we perform the evaluation under moderate attack intensity. For the non-targeted attack, we set the perturbation rate to $\lambda = 0.4$ (covering both feature noise and edge removal). For the targeted attack, we use NETTACK with $p = 1$ perturbation per node for both evasion and poisoning scenarios. All ablated variants adhere to the same evaluation protocol and hyperparameter settings as the full model, ensuring that any observed performance differences are directly and fairly attributable to the specific module that was removed.

Detailed Settings for Section 5.5 (RQ4). To evaluate performance stability, we conduct a sensitivity analysis on four key hyperparameters: the InfoNCE temperature τ , the Information Bottleneck weight λ_{IB} , the MoE regularization weight λ_m , and the uncertainty loss weight λ_u . This analysis is performed on the Cora dataset for 5-shot node classification under a fixed targeted poisoning attack ($p = 1$). We vary one hyperparameter at a time within a predefined range ($\tau \in \{0.1, 0.5, 0.8, 1.0\}$; $\lambda_{IB} \in \{10^{-3}, 10^{-2}, 10^{-1}\}$; $\lambda_m, \lambda_u \in \{0.1, 0.2, 0.5, 1.0\}$) while keeping others at their optimal values to precisely isolate the individual impact of each hyperparameter on the final classification accuracy.

Detailed Settings for Section 5.6 (RQ5). To intuitively demonstrate how SA²GFM learns and adapts representations, we conduct a visualization analysis. We use UMAP to project high-dimensional embeddings into a 2D space for visual inspection and the Silhouette Score to quantitatively measure class clustering quality. We compare embeddings at three key stages: (1) **Pre-trained**, showing general domain features; (2) **Un-finetuned**, revealing initial alignment post-transfer; and (3) **Fine-tuned**, displaying the final task-oriented structure. This analysis is performed in both a cross-dataset (targeting Cora) and a cross-domain (targeting Wiki-CS) scenario to assess adaptability, with nodes colored according to their ground-truth class labels, which allows for a clear visual assessment of the final clustering effectiveness in these settings.

D Additional Results

This section provides more detailed experimental results for RQ1 and RQ2, including the results for each dataset as the target domain under the corresponding attacks.

D.1 Under Non-targeted Feature Attacks

The results presented in Tables D.1, D.2, D.3, and D.4 show that: (1) In the node classification task, SA²GFM consistently achieves state-of-the-art performance across all datasets under both moderate ($\lambda = 0.4$) and high ($\lambda = 0.8$) levels of feature noise. This demonstrates the model’s superior and stable robustness against feature perturbations. (2) When compared to the strongest robust baseline, MDGFM, our model’s performance advantage is particularly evident under high noise conditions. For instance, in the node classification task on ogbn-tech with $\lambda = 0.8$ (Table D.2),

Method	Cora	CiteSeer	PubMed	obgn-Tech	obgn-Home	obgn-arXiv	Wiki-CS
GCN	42.9 \pm 5.8	42.6 \pm 5.5	42.4 \pm 7.1	60.6 \pm 10.6	54.6 \pm 15.3	32.8 \pm 7.5	40.8 \pm 6.7
GAT	45.4 \pm 5.4	53.2 \pm 5.6	46.0 \pm 5.9	64.6 \pm 10.3	58.9 \pm 10.8	40.1 \pm 8.7	45.7 \pm 5.4
DGI	54.6 \pm 6.5	53.6 \pm 4.5	52.3 \pm 5.7	70.2 \pm 7.7	68.1 \pm 9.6	43.4 \pm 5.9	45.1 \pm 5.1
GRAPHCL	52.2 \pm 6.6	54.5 \pm 5.1	48.8 \pm 5.3	73.3 \pm 6.6	68.0 \pm 12.3	42.8 \pm 5.9	48.9 \pm 4.2
GraphPrompt	50.3 \pm 4.8	55.1 \pm 5.3	51.8 \pm 5.6	75.3 \pm 9.4	64.1 \pm 9.3	43.2 \pm 5.6	47.8 \pm 5.0
MDGPT	60.0 \pm 8.1	51.4 \pm 5.0	57.1 \pm 8.1	73.6 \pm 7.3	71.4 \pm 14.7	50.1 \pm 6.1	55.2 \pm 7.5
GCOPE	58.7 \pm 11.0	54.1 \pm 9.0	65.3 \pm 11.3	72.1 \pm 6.5	69.8 \pm 29.1	52.8 \pm 12.1	52.4 \pm 14.7
GraphBridge	62.1 \pm 5.7	57.7 \pm 6.6	60.3 \pm 4.4	76.9 \pm 7.7	70.1 \pm 5.1	55.0 \pm 6.5	58.6 \pm 3.6
MDGFM	65.8 \pm 6.3	60.4 \pm 4.3	65.8 \pm 6.8	83.1 \pm 8.8	73.3 \pm 17.8	59.2 \pm 5.5	61.5 \pm 6.7
SA²GFM (ours)	68.4\pm1.5	62.9\pm4.2	68.8\pm4.4	86.7\pm6.5	76.6\pm5.5	62.8\pm9.4	63.5\pm3.5

Table D.1: Accuracy (%) \pm std. for 20 runs) of **5-shot node classification** under non-targeted feature attack ($\lambda = 0.4$).

Method	Cora	CiteSeer	PubMed	obgn-Tech	obgn-Home	obgn-arXiv	Wiki-CS
GCN	45.9 \pm 9.8	36.3 \pm 5.1	42.3 \pm 9.5	56.0 \pm 12.0	39.5 \pm 9.9	35.7 \pm 5.8	32.2 \pm 7.0
GAT	40.4 \pm 7.5	45.7 \pm 7.2	40.6 \pm 10.0	50.8 \pm 8.4	41.3 \pm 9.4	36.1 \pm 3.9	35.8 \pm 7.1
DGI	46.0 \pm 5.7	44.3 \pm 5.9	42.6 \pm 9.0	56.8 \pm 5.4	45.8 \pm 7.7	35.3 \pm 4.3	39.9 \pm 6.6
GRAPHCL	50.9 \pm 6.0	47.4 \pm 6.6	48.4 \pm 8.4	58.1 \pm 3.9	43.9 \pm 8.9	35.1 \pm 5.4	35.3 \pm 5.6
GraphPrompt	51.6 \pm 7.0	42.5 \pm 6.0	43.5 \pm 7.7	71.3 \pm 8.0	52.3 \pm 13.9	34.7 \pm 4.1	52.0 \pm 5.9
MDGPT	53.3 \pm 8.9	50.1 \pm 4.8	44.5 \pm 6.3	66.4 \pm 7.0	51.7 \pm 24.0	30.1 \pm 5.4	41.9 \pm 8.0
GCOPE	56.8 \pm 10.2	43.4 \pm 10.9	48.2 \pm 11.7	70.0 \pm 21.1	48.8 \pm 23.1	44.1 \pm 5.4	40.5 \pm 10.8
GraphBridge	55.3 \pm 6.8	46.2 \pm 5.4	52.8 \pm 5.3	67.3 \pm 2.8	57.2 \pm 6.3	42.9 \pm 5.6	42.2 \pm 6.9
MDGFM	62.9 \pm 6.2	53.0 \pm 4.7	55.2 \pm 6.1	75.8 \pm 12.8	63.9 \pm 15.9	50.9 \pm 4.7	50.2 \pm 4.9
SA²GFM (ours)	64.2\pm4.9	53.4\pm4.0	57.1\pm1.5	77.9\pm3.6	65.8\pm6.2	54.8\pm1.1	52.8\pm6.7

Table D.2: Accuracy (%) \pm std. for 20 runs) of **5-shot node classification** under non-targeted feature attack ($\lambda = 0.8$).

Method	Cora	CiteSeer	PubMed	obgn-Tech	obgn-Home	obgn-arXiv	Wiki-CS
GCN	51.1 \pm 5.8	41.3 \pm 6.9	61.1 \pm 6.5	67.4 \pm 11.6	60.3 \pm 18.0	41.9 \pm 10.1	43.8 \pm 11.7
GAT	48.1 \pm 5.8	45.5 \pm 7.2	59.3 \pm 5.9	69.0 \pm 10.0	65.8 \pm 7.3	43.8 \pm 8.5	45.1 \pm 4.0
DGI	52.9 \pm 5.2	46.4 \pm 5.3	65.4 \pm 6.2	71.9 \pm 8.3	69.6 \pm 7.6	47.4 \pm 6.8	49.1 \pm 4.8
GRAPHCL	58.5 \pm 5.4	48.1 \pm 5.7	63.8 \pm 6.2	76.9 \pm 6.3	66.4 \pm 8.1	45.3 \pm 6.1	50.5 \pm 3.5
GraphPrompt	57.1 \pm 5.3	43.5 \pm 5.8	55.5 \pm 5.7	73.8 \pm 10.2	70.6 \pm 8.7	48.6 \pm 5.0	60.1 \pm 4.2
MDGPT	64.2 \pm 6.2	55.2 \pm 6.0	62.9 \pm 8.5	79.1 \pm 6.4	64.9 \pm 24.3	52.9 \pm 8.5	53.6 \pm 7.4
GCOPE	63.4 \pm 7.1	52.6 \pm 8.9	59.3 \pm 9.7	81.4 \pm 8.5	72.0 \pm 29.5	56.8 \pm 12.6	54.5 \pm 17.6
GraphBridge	61.0 \pm 4.8	61.0 \pm 7.0	70.9\pm4.2	80.7 \pm 10.6	70.0 \pm 4.9	57.9 \pm 9.4	56.5 \pm 3.6
MDGFM	67.8 \pm 4.9	65.6\pm4.4	67.2 \pm 6.2	85.9\pm7.6	75.6\pm18.9	63.0\pm5.0	62.8\pm4.6
SA²GFM (ours)	69.6\pm5.5	63.9\pm6.3	69.9\pm4.2	87.8\pm9.4	77.8\pm4.5	63.9\pm5.4	64.2\pm6.4

Table D.3: Accuracy (%) \pm std. for 20 runs) of **5-shot graph classification** under non-targeted feature attack ($\lambda = 0.4$).

Method	Cora	CiteSeer	PubMed	obgn-Tech	obgn-Home	obgn-arXiv	Wiki-CS
GCN	40.4 \pm 7.1	37.7 \pm 6.1	50.8 \pm 7.6	63.9 \pm 11.3	54.1 \pm 16.7	33.9 \pm 7.9	40.0 \pm 6.5
GAT	42.1 \pm 7.2	42.8 \pm 5.4	53.8 \pm 5.9	63.1 \pm 10.8	60.5 \pm 8.4	43.1 \pm 8.7	42.9 \pm 5.4
DGI	47.8 \pm 6.9	41.7 \pm 5.9	61.1 \pm 4.8	65.0 \pm 9.0	60.2 \pm 10.1	42.9 \pm 5.9	45.9 \pm 5.5
GRAPHCL	51.9 \pm 5.6	46.3 \pm 6.0	59.8 \pm 6.4	70.1 \pm 7.8	61.2 \pm 10.6	42.0 \pm 6.7	44.2 \pm 3.8
GraphPrompt	50.5 \pm 6.0	41.2 \pm 5.7	50.7 \pm 6.1	67.3 \pm 9.7	67.5 \pm 12.1	43.7 \pm 6.5	57.2 \pm 5.2
MDGPT	55.1 \pm 7.3	50.5 \pm 4.5	58.9 \pm 8.6	75.6 \pm 7.1	64.4 \pm 23.5	45.9 \pm 7.2	47.8 \pm 5.6
GCOPE	59.9 \pm 11.9	53.2 \pm 8.9	55.8 \pm 11.7	73.1 \pm 10.0	67.4 \pm 29.7	52.2 \pm 12.4	48.5 \pm 9.2
GraphBridge	60.8 \pm 6.2	52.8 \pm 6.1	70.9\pm4.9	76.9 \pm 7.7	65.3 \pm 5.7	52.0 \pm 10.1	50.5 \pm 3.6
MDGFM	65.8 \pm 5.6	58.4\pm3.8	65.6 \pm 6.4	83.9\pm9.4	72.1 \pm 18.7	58.6\pm4.9	61.2\pm4.6
SA²GFM (ours)	66.7\pm3.8	60.8\pm9.8	67.0\pm7.0	85.4\pm1.4	74.8\pm7.9	60.9\pm1.0	64.2\pm2.9

Table D.4: Accuracy (%) \pm std. for 20 runs) of **5-shot graph classification** under non-targeted feature attack ($\lambda = 0.8$).

Method	Cora	CiteSeer	PubMed	obgn-Tech	obgn-Home	obgn-arXiv	Wiki-CS
GCN	48.5 \pm 8.5	37.9 \pm 5.8	40.9 \pm 9.8	56.6 \pm 13.2	51.0 \pm 12.9	38.8 \pm 4.7	42.6 \pm 9.9
GAT	52.8 \pm 7.1	42.3 \pm 5.4	44.3 \pm 9.1	55.4 \pm 7.4	53.6 \pm 6.7	41.4 \pm 5.6	46.6 \pm 4.9
DGI	58.4 \pm 5.0	47.1 \pm 6.5	41.3 \pm 7.5	67.6 \pm 2.7	61.0 \pm 6.2	46.6 \pm 4.9	44.1 \pm 7.7
GRAPHCL	53.6 \pm 4.7	49.6 \pm 6.5	48.9 \pm 8.8	68.7 \pm 2.1	48.9 \pm 7.8	43.0 \pm 4.9	49.3 \pm 5.6
GraphPrompt	56.5 \pm 4.4	45.7 \pm 7.0	45.2 \pm 8.1	70.8 \pm 13.3	57.9 \pm 8.4	43.4 \pm 5.2	41.5 \pm 7.1
MDGPT	57.9 \pm 8.2	53.8 \pm 4.7	56.5 \pm 5.5	74.4 \pm 6.7	54.8 \pm 25.1	46.3 \pm 6.7	50.4 \pm 5.0
GCOPE	62.5 \pm 13.0	49.8 \pm 11.4	55.6 \pm 11.4	77.8 \pm 20.2	56.0 \pm 24.3	50.0 \pm 7.2	46.8 \pm 11.8
GraphBridge	55.1 \pm 5.9	50.3 \pm 7.0	52.4 \pm 4.3	76.9 \pm 4.0	62.2 \pm 5.2	47.3 \pm 6.6	47.3 \pm 5.7
MDGFM	65.1 \pm 5.3	54.3 \pm 4.9	58.4 \pm 7.3	81.2 \pm 11.1	65.3 \pm 17.0	55.7 \pm 4.9	52.0 \pm 5.2
SA²GFM (ours)	67.2\pm5.4	56.8\pm2.5	60.2\pm1.4	80.0\pm6.2	69.0\pm5.2	57.8\pm1.4	55.9\pm1.4

Table D.5: Accuracy (% \pm std. for 20 runs) of **5-shot node classification** under non-targeted structure attack ($\lambda = 0.4$).

Method	Cora	CiteSeer	PubMed	obgn-Tech	obgn-Home	obgn-arXiv	Wiki-CS
GCN	44.3 \pm 9.1	33.9 \pm 6.0	36.0 \pm 10.5	51.4 \pm 13.9	43.2 \pm 10.9	35.1 \pm 6.0	37.4 \pm 6.9
GAT	42.8 \pm 6.3	38.1 \pm 5.1	39.9 \pm 8.3	47.8 \pm 7.1	49.1 \pm 8.2	37.6 \pm 4.9	39.5 \pm 4.4
DGI	52.3 \pm 5.6	42.2 \pm 4.8	41.6 \pm 8.1	64.9 \pm 8.1	55.9 \pm 8.7	42.6 \pm 3.7	42.1 \pm 7.4
GRAPHCL	48.3 \pm 5.9	45.0 \pm 5.4	42.2 \pm 7.3	64.6 \pm 5.3	53.4 \pm 8.8	36.4 \pm 5.2	43.6 \pm 5.5
GraphPrompt	52.0 \pm 4.9	41.0 \pm 6.0	41.5 \pm 7.6	65.7 \pm 8.2	54.6 \pm 10.1	39.3 \pm 4.5	42.3 \pm 6.8
MDGPT	52.6 \pm 7.1	48.2 \pm 3.9	51.1 \pm 7.7	67.7 \pm 14.5	50.0 \pm 25.3	46.6 \pm 5.8	46.1 \pm 6.4
GCOPE	59.4 \pm 11.6	43.4 \pm 10.3	45.4 \pm 10.7	71.2 \pm 7.4	51.3 \pm 22.2	47.9 \pm 8.3	43.2 \pm 8.4
GraphBridge	52.6 \pm 6.1	45.2 \pm 6.9	46.4 \pm 9.0	72.1 \pm 5.4	58.6 \pm 6.4	43.1 \pm 6.7	42.7 \pm 6.4
MDGFM	64.5 \pm 6.5	50.7 \pm 4.7	55.7 \pm 6.1	80.9 \pm 12.0	66.1 \pm 22.0	53.2 \pm 5.1	50.3 \pm 4.8
SA²GFM (ours)	63.9\pm7.9	53.5\pm5.8	57.1\pm10.0	77.0\pm9.8	65.9\pm10.9	54.9\pm3.7	53.1\pm7.0

Table D.6: Accuracy (% \pm std. for 20 runs) of **5-shot node classification** under non-targeted structure attack ($\lambda = 0.8$).

Method	Cora	CiteSeer	PubMed	obgn-Tech	obgn-Home	obgn-arXiv	Wiki-CS
GCN	44.9 \pm 8.0	46.4 \pm 5.7	50.9 \pm 5.9	68.7 \pm 12.9	64.4 \pm 13.0	38.4 \pm 9.0	52.6 \pm 10.9
GAT	47.1 \pm 5.3	48.7 \pm 7.8	47.9 \pm 6.3	71.0 \pm 8.4	69.1 \pm 10.8	44.5 \pm 9.2	46.6 \pm 8.2
DGI	49.6 \pm 5.4	54.3 \pm 5.4	52.4 \pm 6.7	71.7 \pm 7.0	66.1 \pm 11.4	45.5 \pm 7.4	52.0 \pm 5.7
GRAPHCL	54.5 \pm 4.6	55.5 \pm 5.8	56.9 \pm 6.5	77.1 \pm 5.2	66.0 \pm 11.3	51.7 \pm 6.6	61.6 \pm 6.3
GraphPrompt	69.0 \pm 5.8	55.9 \pm 6.1	51.4 \pm 5.6	82.9 \pm 9.6	76.8 \pm 9.9	50.5 \pm 6.6	52.3 \pm 6.3
MDGPT	63.5 \pm 6.2	51.1 \pm 4.5	62.7 \pm 7.4	73.3 \pm 8.7	70.7 \pm 21.4	47.1 \pm 6.8	56.0 \pm 8.3
GCOPE	59.2 \pm 10.1	53.2 \pm 8.9	66.8 \pm 12.1	76.3 \pm 11.2	69.8 \pm 30.8	57.5 \pm 12.9	50.1 \pm 17.5
GraphBridge	62.4 \pm 5.0	57.6 \pm 8.2	70.9 \pm 4.9	81.0 \pm 7.5	70.6 \pm 3.0	54.6 \pm 9.2	61.5 \pm 3.6
MDGFM	65.8 \pm 5.6	61.9 \pm 6.3	70.1 \pm 5.2	85.3 \pm 9.7	75.2 \pm 20.6	62.0 \pm 6.0	66.4 \pm 5.2
SA²GFM (ours)	69.5\pm6.5	64.0\pm3.3	69.9\pm4.4	87.7\pm9.5	77.9\pm2.3	63.9\pm6.4	64.3\pm8.5

Table D.7: Accuracy (% \pm std. for 20 runs) of **5-shot graph classification** under non-targeted structure attack ($\lambda = 0.4$).

Method	Cora	CiteSeer	PubMed	obgn-Tech	obgn-Home	obgn-arXiv	Wiki-CS
GCN	40.9 \pm 6.9	39.8 \pm 6.2	45.2 \pm 9.7	65.5 \pm 13.7	52.4 \pm 21.4	32.8 \pm 5.8	46.2 \pm 9.9
GAT	48.8 \pm 6.9	44.7 \pm 6.0	42.2 \pm 8.6	69.1 \pm 10.8	63.8 \pm 12.1	41.3 \pm 8.7	42.0 \pm 5.6
DGI	49.3 \pm 6.8	48.9 \pm 5.9	47.3 \pm 8.1	68.4 \pm 8.0	64.4 \pm 11.1	42.8 \pm 7.3	42.4 \pm 3.8
GRAPHCL	51.0 \pm 6.0	46.6 \pm 6.0	51.0 \pm 8.3	73.6 \pm 7.9	63.0 \pm 11.1	46.2 \pm 5.8	51.4 \pm 3.4
GraphPrompt	65.3 \pm 6.6	48.2 \pm 6.0	46.7 \pm 8.4	81.3 \pm 10.6	69.4 \pm 9.9	42.9 \pm 4.7	49.7 \pm 6.9
MDGPT	59.8 \pm 6.5	43.7 \pm 7.1	55.9 \pm 8.6	68.0 \pm 7.1	63.1 \pm 23.5	42.3 \pm 6.8	48.9 \pm 7.0
GCOPE	55.1 \pm 11.9	49.6 \pm 10.9	59.5 \pm 11.7	72.0 \pm 10.0	64.2 \pm 28.4	51.5 \pm 8.3	42.6 \pm 10.8
GraphBridge	58.4 \pm 6.8	52.1 \pm 5.4	58.3 \pm 5.3	77.4 \pm 7.3	65.2 \pm 6.3	50.8 \pm 10.6	58.5 \pm 3.6
MDGFM	64.0 \pm 6.2	59.9 \pm 3.8	68.8 \pm 6.4	82.0 \pm 12.7	72.0 \pm 18.7	60.5 \pm 4.9	65.5 \pm 7.4
SA²GFM (ours)	66.6\pm11.1	60.7\pm9.8	67.1\pm6.9	84.8\pm4.9	74.7\pm8.9	61.1\pm6.7	61.2\pm2.9

Table D.8: Accuracy (% \pm std. for 20 runs) of **5-shot graph classification** under non-targeted structure attack ($\lambda = 0.8$).

Method	Cora	CiteSeer	PubMed	obgn-Tech	obgn-Home	obgn-arXiv	Wiki-CS
GCN	44.8 \pm 8.0	36.0 \pm 7.4	43.6 \pm 12.1	62.1 \pm 15.4	49.4 \pm 13.2	38.2 \pm 5.0	36.2 \pm 7.6
GAT	42.2 \pm 7.6	42.5 \pm 5.1	40.8 \pm 11.1	63.2 \pm 8.7	50.3 \pm 6.9	39.1 \pm 5.4	36.0 \pm 6.1
DGI	46.6 \pm 6.5	48.4 \pm 4.5	45.0 \pm 9.9	76.0 \pm 5.7	60.1 \pm 7.4	45.5 \pm 5.4	46.3 \pm 7.5
GRAPHCL	52.0 \pm 6.0	49.0 \pm 4.7	51.8 \pm 10.3	66.3 \pm 4.8	57.4 \pm 8.6	42.5 \pm 4.8	41.8 \pm 6.1
GraphPrompt	44.0 \pm 7.0	46.6 \pm 5.1	54.3 \pm 8.8	69.8 \pm 7.3	57.3 \pm 9.6	46.8 \pm 6.0	43.1 \pm 5.9
MDGPT	57.3 \pm 7.9	43.4 \pm 5.8	49.8 \pm 5.8	73.6 \pm 6.1	51.8 \pm 24.8	47.8 \pm 5.8	49.6 \pm 8.4
GCOPE	54.7 \pm 10.0	49.3 \pm 8.1	52.2 \pm 10.7	76.4 \pm 20.9	60.7 \pm 24.3	52.3 \pm 7.0	47.1 \pm 10.5
GraphBridge	53.6 \pm 6.8	50.9 \pm 8.8	56.6 \pm 9.5	74.6 \pm 6.0	63.5 \pm 3.6	53.6 \pm 6.0	44.6 \pm 9.3
MDGFM	64.2 \pm 5.4	54.9 \pm 5.4	58.2 \pm 6.8	78.1 \pm 14.7	67.3 \pm 16.8	58.6 \pm 5.7	53.3 \pm 5.8
SA²GFM (ours)	67.1\pm4.4	56.6\pm3.5	60.1\pm7.2	81.3\pm4.1	69.0\pm1.7	57.9\pm5.2	55.9\pm9.7

Table D.9: Accuracy (%) \pm std. for 20 runs) of **5-shot node classification** under targeted evasion attack ($p = 1$).

Method	Cora	CiteSeer	PubMed	obgn-Tech	obgn-Home	obgn-arXiv	Wiki-CS
GCN	42.4 \pm 7.4	33.1 \pm 6.7	37.7 \pm 7.0	64.4 \pm 10.8	54.1 \pm 14.6	33.1 \pm 6.5	43.1 \pm 8.2
GAT	47.6 \pm 5.6	49.6 \pm 5.7	47.3 \pm 6.6	60.2 \pm 9.2	56.8 \pm 10.3	45.2 \pm 8.8	47.1 \pm 6.2
DGI	50.3 \pm 5.7	52.0 \pm 4.5	49.9 \pm 6.6	63.2 \pm 8.0	67.0 \pm 9.7	44.3 \pm 5.6	49.5 \pm 4.9
GRAPHCL	43.2 \pm 5.7	53.1 \pm 4.7	50.8 \pm 6.2	73.7 \pm 6.8	62.9 \pm 12.0	51.4 \pm 5.6	42.2 \pm 4.7
GraphPrompt	50.3 \pm 4.9	44.9 \pm 5.4	48.3 \pm 6.3	71.4 \pm 9.4	61.1 \pm 9.3	44.0 \pm 5.0	47.6 \pm 5.5
MDGPT	56.5 \pm 7.6	41.5 \pm 6.2	56.5 \pm 10.1	70.6 \pm 8.0	66.6 \pm 15.9	47.4 \pm 5.6	51.2 \pm 7.5
GCOPE	55.9 \pm 10.5	49.6 \pm 10.2	55.2 \pm 12.3	72.8 \pm 18.2	50.4 \pm 29.6	45.6 \pm 12.4	46.1 \pm 14.2
GraphBridge	56.4 \pm 5.3	53.4 \pm 6.1	50.2 \pm 6.5	83.3 \pm 7.5	63.1 \pm 5.8	48.9 \pm 6.8	56.5 \pm 3.6
MDGFM	63.4 \pm 6.6	58.9 \pm 4.8	58.2 \pm 6.3	80.1 \pm 7.4	77.3 \pm 20.1	58.7 \pm 4.9	60.5 \pm 4.5
SA²GFM (ours)	66.3\pm7.8	60.6\pm4.6	66.4\pm3.9	84.6\pm11.8	74.5\pm5.7	60.8\pm7.8	61.5\pm3.8

Table D.10: Accuracy (%) \pm std. for 20 runs) of **5-shot node classification** under targeted evasion attack ($p = 2$).

Method	Cora	CiteSeer	PubMed	obgn-Tech	obgn-Home	obgn-arXiv	Wiki-CS
GCN	44.0 \pm 6.9	33.2 \pm 5.9	36.7 \pm 11.0	51.4 \pm 16.3	47.8 \pm 13.6	36.6 \pm 5.3	33.8 \pm 7.6
GAT	52.3 \pm 6.7	43.1 \pm 6.6	37.5 \pm 8.6	52.4 \pm 8.9	46.5 \pm 6.3	34.6 \pm 6.7	34.4 \pm 5.6
DGI	44.7 \pm 4.4	45.5 \pm 4.7	42.1 \pm 7.6	56.0 \pm 7.1	54.0 \pm 4.9	36.7 \pm 5.4	41.1 \pm 6.5
GRAPHCL	42.1 \pm 5.7	40.7 \pm 7.3	42.7 \pm 7.8	55.8 \pm 6.7	55.9 \pm 6.6	37.8 \pm 4.5	42.4 \pm 6.1
GraphPrompt	52.9 \pm 6.9	42.8 \pm 6.3	45.3 \pm 7.5	68.4 \pm 8.9	55.3 \pm 8.3	39.0 \pm 4.7	39.4 \pm 8.1
MDGPT	60.6 \pm 7.0	56.4 \pm 4.7	62.2 \pm 6.4	59.9 \pm 6.7	54.0 \pm 24.1	45.6 \pm 5.3	49.5 \pm 8.9
GCOPE	55.0 \pm 10.4	39.5 \pm 6.8	48.7 \pm 10.9	62.6 \pm 20.8	55.6 \pm 24.2	39.1 \pm 5.9	42.1 \pm 10.6
GraphBridge	53.8 \pm 5.5	47.4 \pm 7.9	44.0 \pm 10.1	66.0 \pm 7.0	57.1 \pm 3.7	47.6 \pm 6.2	43.3 \pm 10.1
MDGFM	61.9 \pm 6.8	54.1\pm4.5	53.4 \pm 7.3	78.3\pm17.1	62.9 \pm 15.3	50.8 \pm 5.0	50.2 \pm 6.2
SA²GFM (ours)	63.8\pm4.7	53.6\pm2.9	56.8\pm9.8	77.9\pm4.9	65.9\pm2.7	55.1\pm5.8	53.3\pm4.9

Table D.11: Accuracy (%) \pm std. for 20 runs) of **5-shot node classification** under targeted evasion attack ($p = 3$).

SA²GFM achieves an accuracy of 77.9%, significantly outperforming MDGFM's 75.8%. This consistent superiority suggests that our structure-aware semantic augmentation and information bottleneck mechanism are highly effective at preserving essential information and filtering noise when node features are severely corrupted. ③ While all models experience performance degradation as the noise level increases from $\lambda = 0.4$ to $\lambda = 0.8$, SA²GFM exhibits a more graceful decline, maintaining its top-ranking position and widening the performance gap with other baselines. This resilience is critical in real-world scenarios where data quality varies, highlighting our approach's practical value. The experimental results for the graph classification task (Ta-

bles D.3 and D.4) show a similar trend, further corroborating the robustness and effectiveness of our proposed method.

D.2 Under Non-targeted Structure Attacks

The results presented in Tables D.5, D.6, D.7, and D.8 show that: ① For the node classification task, SA²GFM maintains its top-tier performance across all datasets when subjected to random structural perturbations. Even with a high proportion of edges removed ($\lambda = 0.8$), our model consistently outperforms all baselines, showcasing its exceptional structural robustness. ② The advantage of our model is especially clear when compared with MDGFM. For example, on the obgn-arxiv dataset with $\lambda = 0.8$ (Table D.6),

Method	Cora	CiteSeer	PubMed	obgn-Tech	obgn-Home	obgn-arXiv	Wiki-CS
GCN	47.9 \pm 6.1	48.7 \pm 6.0	47.4 \pm 7.3	69.8 \pm 10.6	64.6 \pm 15.6	38.8 \pm 6.1	47.0 \pm 6.7
GAT	50.2 \pm 5.8	53.2 \pm 5.7	52.2 \pm 5.9	68.9 \pm 10.2	69.0 \pm 11.2	45.1 \pm 8.5	47.9 \pm 5.5
DGI	57.4 \pm 6.5	53.7 \pm 4.9	60.4 \pm 5.6	76.6 \pm 7.8	68.0 \pm 9.8	45.8 \pm 6.0	50.3 \pm 5.0
GRAPHCL	56.1 \pm 6.5	55.0 \pm 4.7	51.8 \pm 5.4	74.0 \pm 6.5	67.4 \pm 12.3	51.7 \pm 5.3	54.8 \pm 4.3
GraphPrompt	55.8 \pm 4.9	59.1 \pm 5.5	53.9 \pm 5.6	71.5 \pm 9.2	70.9 \pm 9.2	42.8 \pm 5.4	52.1 \pm 4.9
MDGPT	60.6 \pm 8.2	56.4 \pm 4.7	62.2 \pm 8.2	76.4 \pm 7.6	72.8 \pm 15.2	53.2 \pm 6.1	58.3 \pm 7.5
GCOPE	64.0 \pm 10.9	58.2 \pm 9.1	69.1 \pm 11.4	84.2 \pm 7.0	72.5 \pm 28.9	57.6 \pm 12.3	57.3 \pm 14.7
GraphBridge	63.9 \pm 5.6	62.3 \pm 6.8	57.5 \pm 4.5	82.3 \pm 7.4	67.2 \pm 5.2	59.7 \pm 6.9	58.5 \pm 3.6
MDGFM	68.8 \pm 6.7	66.6\pm4.1	68.0 \pm 6.9	85.9 \pm 8.8	76.3 \pm 17.8	63.1 \pm 5.5	62.6 \pm 6.8
SA²GFM (ours)	70.0\pm1.4	<u>65.0\pm8.2</u>	70.8\pm5.4	88.8\pm3.4	78.4\pm3.5	64.8\pm9.4	65.4\pm5.5

Table D.12: Accuracy (% \pm std. for 20 runs) of **5-shot graph classification** under targeted evasion attack ($p = 1$).

Method	Cora	CiteSeer	PubMed	obgn-Tech	obgn-Home	obgn-arXiv	Wiki-CS
GCN	46.8 \pm 5.8	47.9 \pm 5.6	46.6 \pm 7.1	63.6 \pm 10.6	63.9 \pm 15.2	34.9 \pm 7.1	43.8 \pm 6.6
GAT	49.1 \pm 5.7	53.3 \pm 5.7	48.1 \pm 5.9	68.7 \pm 10.3	68.5 \pm 10.7	45.4 \pm 8.9	50.8 \pm 5.5
DGI	58.0 \pm 6.4	53.5 \pm 4.7	57.4 \pm 5.8	72.6 \pm 7.8	68.1 \pm 9.9	45.6 \pm 6.3	51.2 \pm 5.1
GRAPHCL	57.1 \pm 6.5	54.8 \pm 4.8	51.7 \pm 5.5	74.0 \pm 6.6	67.3 \pm 12.1	47.3 \pm 5.6	54.8 \pm 4.2
GraphPrompt	59.8 \pm 4.8	55.0 \pm 5.4	53.8 \pm 5.7	81.3 \pm 9.4	73.9 \pm 9.3	43.2 \pm 5.3	49.0 \pm 5.0
MDGPT	61.4 \pm 8.0	52.3 \pm 4.6	62.1 \pm 8.2	77.4 \pm 7.4	72.2 \pm 14.4	52.1 \pm 6.1	55.2 \pm 7.5
GCOPE	64.1 \pm 11.1	58.5 \pm 9.1	70.3\pm11.3	75.7 \pm 6.7	70.3 \pm 28.8	53.1 \pm 12.0	52.3 \pm 14.8
GraphBridge	63.0 \pm 5.7	60.7 \pm 6.7	63.4 \pm 4.4	80.1 \pm 7.3	73.1 \pm 5.0	57.5 \pm 6.4	60.6 \pm 3.6
MDGFM	67.0 \pm 6.6	<u>62.4\pm4.3</u>	66.0 \pm 6.8	<u>86.0\pm9.0</u>	<u>76.2\pm17.7</u>	<u>60.1\pm5.4</u>	<u>62.6\pm6.8</u>
SA²GFM (ours)	69.4\pm7.5	64.0\pm6.0	<u>69.8\pm7.4</u>	87.9\pm9.4	77.5\pm9.5	63.7\pm5.4	64.6\pm6.5

Table D.13: Accuracy (% \pm std. for 20 runs) of **5-shot graph classification** under targeted evasion attack ($p = 2$).

Method	Cora	CiteSeer	PubMed	obgn-Tech	obgn-Home	obgn-arXiv	Wiki-CS
GCN	42.9 \pm 5.8	42.6 \pm 5.5	42.4 \pm 7.1	60.6 \pm 10.6	54.6 \pm 15.3	32.8 \pm 7.5	40.8 \pm 6.7
GAT	45.4 \pm 5.4	53.2 \pm 5.6	46.0 \pm 5.9	64.6 \pm 10.3	58.9 \pm 10.8	40.1 \pm 8.7	45.7 \pm 5.4
DGI	54.6 \pm 6.5	53.6 \pm 4.5	52.3 \pm 5.7	70.2 \pm 7.7	68.1 \pm 9.6	43.4 \pm 5.9	45.1 \pm 5.1
GRAPHCL	52.2 \pm 6.6	54.5 \pm 5.1	48.8 \pm 5.3	73.3 \pm 6.6	68.0 \pm 12.3	42.8 \pm 5.9	48.9 \pm 4.2
GraphPrompt	50.3 \pm 4.8	55.1 \pm 5.3	51.8 \pm 5.6	75.3 \pm 9.4	64.1 \pm 9.3	43.2 \pm 5.6	47.8 \pm 5.0
MDGPT	60.0 \pm 8.1	51.4 \pm 5.0	57.1 \pm 8.1	73.6 \pm 7.3	71.4 \pm 14.7	50.1 \pm 6.1	55.2 \pm 7.5
GCOPE	58.7 \pm 11.0	54.1 \pm 9.0	<u>65.3\pm11.3</u>	72.1 \pm 6.5	69.8 \pm 29.1	52.8 \pm 12.1	52.4 \pm 14.7
GraphBridge	62.1 \pm 5.7	57.7 \pm 6.6	60.3 \pm 4.4	76.9 \pm 7.7	70.1 \pm 5.1	55.0 \pm 6.5	58.6 \pm 3.6
MDGFM	<u>65.8\pm6.3</u>	<u>60.4\pm4.3</u>	<u>65.8\pm6.8</u>	<u>83.1\pm8.8</u>	<u>73.3\pm17.8</u>	<u>59.2\pm5.5</u>	<u>61.5\pm6.7</u>
SA²GFM (ours)	68.4\pm1.5	62.9\pm4.2	68.8\pm4.4	86.7\pm6.5	76.6\pm5.5	62.8\pm9.4	63.5\pm3.5

Table D.14: Accuracy (% \pm std. for 20 runs) of **5-shot graph classification** under targeted evasion attack ($p = 3$).

SA²GFM achieves an accuracy of 53.2%, which is a notable improvement over MDGFM’s 50.9%. This indicates that our hierarchical structure optimization module is more effective at recovering and preserving crucial topological information than the GSL methods used in other baselines. ③ As the structural noise intensifies from $\lambda = 0.4$ to $\lambda = 0.8$, the performance of most models drops significantly. However, SA²GFM demonstrates a more resilient performance, with a smaller accuracy decrease compared to its competitors. The results from the graph classification experiments (Tables D.7 and D.8) further validate these findings, confirming the superior structural robustness of our approach.

D.3 Under Targeted Evasion Attacks

The results presented in Tables D.9 to D.14 show that: ① In the node classification task, SA²GFM demonstrates remarkable robustness against targeted evasion attacks, consistently outperforming all baselines across every dataset and at all attack intensities ($p = 1, 2, 3$). This underscores its strong defensive capabilities against strategic adversarial perturbations. ② The performance gap between SA²GFM and the strongest baseline, MDGFM, widens as the attack becomes more severe. For instance, under the most intense attack ($p = 3$) on the obgn-arxiv dataset (Table D.11), SA²GFM achieves 50.1% accuracy, whereas MDGFM drops to 45.6%. This highlights the effectiveness of our expert

Method	Cora	CiteSeer	PubMed	obgn-Tech	obgn-Home	obgn-arXiv	Wiki-CS
GCN	49.5 \pm 5.5	37.0 \pm 6.9	51.7 \pm 12.4	69.8 \pm 12.0	51.4 \pm 10.4	30.3 \pm 5.5	49.4 \pm 6.6
GAT	50.2 \pm 7.5	46.5 \pm 4.3	49.0 \pm 8.9	71.2 \pm 8.9	61.6 \pm 7.3	39.1 \pm 4.9	51.5 \pm 6.7
DGI	53.3 \pm 6.8	45.8 \pm 4.9	46.2 \pm 8.6	70.2 \pm 4.7	59.9 \pm 6.3	46.4 \pm 3.9	45.1 \pm 6.4
GRAPHCL	57.2 \pm 6.5	47.1 \pm 6.3	56.6 \pm 8.7	71.2 \pm 4.6	58.4 \pm 6.7	42.9 \pm 4.9	49.8 \pm 6.2
GraphPrompt	56.7 \pm 5.7	40.2 \pm 7.0	45.5 \pm 7.2	78.8 \pm 10.0	58.1 \pm 11.5	46.3 \pm 4.7	51.9 \pm 8.0
MDGPT	54.5 \pm 7.5	43.5 \pm 2.9	56.6 \pm 5.2	75.8 \pm 6.1	61.3 \pm 14.7	53.4 \pm 5.8	51.4 \pm 7.0
GCOPE	58.8 \pm 12.0	48.8 \pm 9.6	52.7 \pm 13.1	79.2 \pm 7.0	59.6 \pm 26.1	51.5 \pm 7.2	47.1 \pm 12.1
GraphBridge	59.7 \pm 6.8	45.2 \pm 8.5	52.2 \pm 6.5	78.1 \pm 3.8	62.3 \pm 3.7	54.7 \pm 5.0	50.3 \pm 7.2
MDGFM	63.5 \pm 7.7	53.5 \pm 4.6	57.4 \pm 7.2	83.2 \pm 13.6	67.8 \pm 13.7	56.1 \pm 3.6	55.2 \pm 5.1
SA²GFM (ours)	66.4\pm6.5	55.6\pm4.6	59.5\pm6.5	80.4\pm4.1	68.3\pm3.5	57.1\pm6.6	53.2\pm2.5

Table D.15: Accuracy (% \pm std. for 20 runs) of **5-shot node classification** under targeted poisoning attack ($p = 1$).

Method	Cora	CiteSeer	PubMed	obgn-Tech	obgn-Home	obgn-arXiv	Wiki-CS
GCN	48.1 \pm 9.0	36.4 \pm 4.8	38.9 \pm 11.9	58.8 \pm 13.7	48.4 \pm 10.2	34.8 \pm 5.0	47.3 \pm 7.6
GAT	59.0 \pm 6.2	44.5 \pm 5.2	42.0 \pm 9.0	62.2 \pm 8.8	59.1 \pm 7.0	31.9 \pm 4.5	45.2 \pm 5.6
DGI	57.5 \pm 6.1	45.9 \pm 4.5	43.3 \pm 9.3	66.5 \pm 4.7	55.4 \pm 7.9	45.7 \pm 5.1	43.8 \pm 6.9
GRAPHCL	47.2 \pm 5.9	42.9 \pm 5.1	43.9 \pm 8.5	67.6 \pm 3.1	56.5 \pm 8.5	32.0 \pm 5.4	45.2 \pm 5.7
GraphPrompt	50.2 \pm 7.0	42.8 \pm 5.7	47.9 \pm 7.5	69.0 \pm 10.7	56.6 \pm 7.1	43.1 \pm 4.8	40.4 \pm 5.6
MDGPT	60.6 \pm 8.0	52.8 \pm 5.0	51.7 \pm 7.1	74.3 \pm 6.9	62.6 \pm 12.5	48.6 \pm 5.4	39.9 \pm 7.6
GCOPE	55.0 \pm 12.2	49.0 \pm 8.5	47.0 \pm 10.9	71.1 \pm 7.8	55.4 \pm 23.4	49.2 \pm 7.3	42.2 \pm 11.1
GraphBridge	59.1 \pm 6.3	43.7 \pm 6.6	50.5 \pm 5.3	76.1 \pm 5.4	60.9 \pm 5.7	45.4 \pm 5.4	44.8 \pm 7.7
MDGFM	62.5 \pm 7.1	55.2 \pm 3.9	53.4 \pm 7.5	74.9 \pm 15.4	68.6 \pm 17.1	51.5 \pm 5.9	50.0 \pm 6.4
SA²GFM (ours)	64.3\pm1.9	54.0\pm4.8	57.4\pm3.8	77.1\pm5.9	66.3\pm4.7	54.3\pm3.8	52.7\pm9.7

Table D.16: Accuracy (% \pm std. for 20 runs) of **5-shot node classification** under targeted poisoning attack ($p = 2$).

Method	Cora	CiteSeer	PubMed	obgn-Tech	obgn-Home	obgn-arXiv	Wiki-CS
GCN	44.4 \pm 4.7	34.0 \pm 5.5	32.4 \pm 9.9	57.8 \pm 12.8	46.4 \pm 13.4	38.3 \pm 6.0	38.5 \pm 8.8
GAT	52.4 \pm 6.9	42.6 \pm 5.6	38.3 \pm 8.3	54.4 \pm 7.8	56.0 \pm 7.7	38.5 \pm 5.4	37.6 \pm 6.7
DGI	47.8 \pm 6.0	45.2 \pm 5.9	35.9 \pm 8.9	55.4 \pm 6.0	51.1 \pm 10.6	44.8 \pm 4.5	45.9 \pm 5.1
GRAPHCL	48.9 \pm 5.1	41.3 \pm 5.3	37.6 \pm 7.6	67.6 \pm 3.4	53.0 \pm 9.1	30.0 \pm 5.5	41.3 \pm 4.7
GraphPrompt	45.6 \pm 6.1	42.6 \pm 4.6	39.6 \pm 6.1	63.9 \pm 6.2	53.5 \pm 6.6	42.0 \pm 4.0	32.5 \pm 7.7
MDGPT	60.6 \pm 8.0	52.8 \pm 5.0	51.7 \pm 7.1	74.3 \pm 6.9	62.6 \pm 12.5	48.6 \pm 5.4	39.9 \pm 7.6
GCOPE	56.8 \pm 10.4	49.0 \pm 8.5	47.0 \pm 10.9	71.1 \pm 7.8	55.4 \pm 23.4	49.2 \pm 7.3	42.2 \pm 11.1
GraphBridge	54.8 \pm 5.6	43.9 \pm 8.1	50.5 \pm 7.4	76.1 \pm 5.4	61.3 \pm 6.6	44.5 \pm 6.0	42.4 \pm 8.3
MDGFM	61.4 \pm 7.8	55.2 \pm 4.8	50.8 \pm 5.2	72.4 \pm 13.7	62.1 \pm 16.2	50.4 \pm 4.7	46.4 \pm 5.7
SA²GFM (ours)	62.3\pm1.4	51.5\pm1.1	54.6\pm1.2	74.8\pm1.0	64.0\pm1.3	52.9\pm1.2	50.7\pm1.2

Table D.17: Accuracy (% \pm std. for 20 runs) of **5-shot node classification** under targeted poisoning attack ($p = 3$).

routing and structural optimization in preserving performance even when the adversary has more power. ③ As the number of perturbations increases, all models show a decline in accuracy, but SA²GFM’s performance degrades more slowly and gracefully than its counterparts. This trend of superior stability is also reflected in the graph classification results (Tables D.12 to D.14), further confirming that our model’s robustness is consistent across different tasks.

D.4 Under Targeted Poisoning Attacks

The results presented in Tables D.15 to D.20 show that: ① SA²GFM shows exceptional robustness against targeted

poisoning attacks, consistently leading in performance for node classification across all datasets and attack levels ($p = 1, 2, 3$). This proves its ability to learn reliable representations even from corrupted training data. ② The model’s advantage over the strongest baseline, MDGFM, is significant. For example, in the most severe attack scenario ($p = 3$) on the Wiki-CS dataset (Table D.17), SA²GFM achieves 50.7% accuracy, while MDGFM’s performance degrades to 46.4%. This suggests that our pre-training strategy, which distills robust patterns via the information bottleneck, and the hierarchical fine-tuning are crucial for defending against poisoning. ③ As the poisoning

Method	Cora	CiteSeer	PubMed	obgn-Tech	obgn-Home	obgn-arXiv	Wiki-CS
GCN	46.5 \pm 7.6	38.9 \pm 6.9	38.3 \pm 6.1	69.2 \pm 10.4	59.2 \pm 18.2	35.0 \pm 5.7	45.6 \pm 10.1
GAT	49.1 \pm 5.5	51.0 \pm 5.2	47.6 \pm 6.6	69.1 \pm 10.4	58.3 \pm 10.7	46.0 \pm 7.5	40.8 \pm 5.6
DGI	51.3 \pm 6.8	53.1 \pm 6.5	57.8 \pm 6.6	72.9 \pm 8.6	67.5 \pm 10.7	45.8 \pm 5.8	50.8 \pm 4.6
GRAPHCL	43.9 \pm 5.4	53.8 \pm 6.8	49.8 \pm 6.1	74.8 \pm 5.8	65.3 \pm 13.7	52.3 \pm 7.1	43.9 \pm 4.9
GraphPrompt	51.1 \pm 6.0	55.1 \pm 5.5	49.1 \pm 6.9	81.4 \pm 9.2	61.6 \pm 11.7	44.8 \pm 6.0	48.2 \pm 4.8
MDGPT	52.1 \pm 6.4	53.3 \pm 4.9	58.4 \pm 5.7	72.6 \pm 7.5	67.2 \pm 22.8	53.4 \pm 6.1	54.1 \pm 6.8
GCOPE	49.1 \pm 7.2	51.3 \pm 8.7	56.2 \pm 9.0	86.3 \pm 12.2	51.6 \pm 28.3	50.4 \pm 11.8	53.4 \pm 12.4
GraphBridge	57.2 \pm 6.0	61.8 \pm 5.8	54.8 \pm 6.7	83.5 \pm 8.0	65.6 \pm 6.2	56.7 \pm 9.3	58.6 \pm 3.6
MDGFM	64.9 \pm 4.4	60.4 \pm 4.4	67.1 \pm 7.0	80.0 \pm 7.2	73.8 \pm 18.1	60.0 \pm 5.6	61.0 \pm 5.6
SA²GFM (ours)	68.9\pm4.4	63.5\pm5.5	69.1\pm7.6	87.0\pm4.5	77.0\pm7.5	63.2\pm8.5	63.4\pm3.5

Table D.18: Accuracy (%) \pm std. for 20 runs of **5-shot graph classification** under targeted poisoning attack ($p = 1$).

Method	Cora	CiteSeer	PubMed	obgn-Tech	obgn-Home	obgn-arXiv	Wiki-CS
GCN	46.8 \pm 8.1	38.1 \pm 6.4	37.6 \pm 7.0	64.4 \pm 10.8	54.1 \pm 14.6	33.2 \pm 6.5	43.1 \pm 8.2
GAT	47.6 \pm 5.6	49.6 \pm 5.7	47.3 \pm 6.6	60.2 \pm 9.2	56.8 \pm 10.3	45.1 \pm 8.8	47.1 \pm 6.2
DGI	50.3 \pm 5.7	52.0 \pm 4.7	49.9 \pm 6.6	63.3 \pm 8.0	67.0 \pm 9.7	44.3 \pm 5.6	49.5 \pm 4.9
GRAPHCL	43.1 \pm 5.7	53.1 \pm 4.7	50.8 \pm 6.2	73.7 \pm 6.8	62.8 \pm 12.0	51.3 \pm 5.6	42.2 \pm 4.7
GraphPrompt	50.3 \pm 4.9	44.9 \pm 5.4	48.3 \pm 6.3	71.4 \pm 9.4	61.1 \pm 9.3	44.0 \pm 5.0	47.6 \pm 5.5
MDGPT	51.5 \pm 7.6	41.5 \pm 6.2	56.5 \pm 10.1	70.6 \pm 8.0	66.6 \pm 15.9	47.4 \pm 5.6	51.2 \pm 7.5
GCOPE	50.0 \pm 9.4	49.6 \pm 10.2	55.2 \pm 12.3	72.8 \pm 18.2	50.4 \pm 29.7	45.6 \pm 12.4	46.1 \pm 14.2
GraphBridge	56.4 \pm 5.3	53.4 \pm 6.1	50.2 \pm 6.5	83.3 \pm 7.5	63.1 \pm 5.8	48.9 \pm 6.8	56.5 \pm 3.6
MDGFM	63.4 \pm 6.6	58.9 \pm 4.8	58.2 \pm 6.3	80.1 \pm 7.4	77.2 \pm 20.1	58.7 \pm 4.9	60.5 \pm 4.5
SA²GFM (ours)	66.3\pm7.9	60.6\pm4.6	66.4\pm3.9	84.6\pm11.8	74.5\pm5.7	60.9\pm7.8	61.4\pm3.8

Table D.19: Accuracy (%) \pm std. for 20 runs of **5-shot graph classification** under targeted poisoning attack ($p = 2$).

Method	Cora	CiteSeer	PubMed	obgn-Tech	obgn-Home	obgn-arXiv	Wiki-CS
GCN	42.3 \pm 7.4	35.1 \pm 6.1	38.3 \pm 5.4	59.2 \pm 9.8	52.9 \pm 16.7	35.7 \pm 5.8	41.4 \pm 9.6
GAT	48.2 \pm 6.8	39.4 \pm 5.0	37.6 \pm 5.4	59.1 \pm 9.7	56.5 \pm 8.4	42.2 \pm 7.7	48.8 \pm 5.7
DGI	50.7 \pm 5.1	46.2 \pm 5.2	50.6 \pm 5.1	62.9 \pm 7.4	56.1 \pm 7.3	42.4 \pm 5.2	49.0 \pm 4.5
GRAPHCL	43.9 \pm 5.5	42.9 \pm 4.7	46.5 \pm 5.7	54.0 \pm 6.8	62.3 \pm 8.9	49.5 \pm 4.9	43.1 \pm 3.7
GraphPrompt	50.8 \pm 4.8	45.0 \pm 5.3	45.3 \pm 5.6	61.1 \pm 9.4	59.3 \pm 7.6	41.2 \pm 4.9	47.2 \pm 5.0
MDGPT	53.9 \pm 6.1	40.6 \pm 5.5	54.3 \pm 8.4	68.8 \pm 8.9	67.7 \pm 15.6	43.8 \pm 6.3	49.0 \pm 8.3
GCOPE	58.5 \pm 8.3	50.0 \pm 9.7	59.3 \pm 8.8	79.6 \pm 6.6	51.6 \pm 26.6	46.5 \pm 9.7	40.1 \pm 10.6
GraphBridge	56.6 \pm 5.0	51.9 \pm 5.2	55.4 \pm 6.1	73.8 \pm 7.0	61.4 \pm 6.9	42.9 \pm 7.7	48.6 \pm 3.6
MDGFM	62.6 \pm 5.8	55.2 \pm 5.6	62.9 \pm 6.6	83.5 \pm 9.6	69.3 \pm 18.1	56.7 \pm 6.1	56.5 \pm 8.0
SA²GFM (ours)	64.6\pm1.4	58.7\pm1.3	64.5\pm1.3	82.6\pm1.4	73.1\pm1.5	58.1\pm1.2	59.0\pm1.2

Table D.20: Accuracy (%) \pm std. for 20 runs of **5-shot graph classification** under targeted poisoning attack ($p = 3$).

attack intensifies, SA²GFM demonstrates superior stability with a more graceful performance decline compared to other baselines. This resilience is further confirmed by the graph classification results (Tables D.18 to D.20), which exhibit the same trend of robust and superior performance.

E Related Work Discussions

E.1 Multi-domain Graph Foundation Models

Multi-domain graph pre-training is a cornerstone for developing general-purpose Graph Foundation Models (GFMs), aiming to distill transferable knowledge from diverse domains (Yu et al. 2024; Yuan et al. 2025b). Addressing the

domain gap is a central challenge, with existing methods focusing on either feature or structure-level alignment.

Feature-level alignment aims to unify heterogeneous semantic spaces. For instance, MDGPT (Yu et al. 2024) introduces learnable domain tokens to adjust features from each source domain. In contrast, BRIDGE (Yuan et al. 2025b) employs domain-invariant aligners to extract generalizable representations and provides a theoretical upper bound on the generalization error. Other works have also explored leveraging language models for alignment, though these are often limited to text-attributed graphs (Tang et al. 2024). **Structure-level alignment** directly addresses topological

discrepancies. A representative work, MDGFM (Wang et al. 2025), integrates Graph Structure Learning (GSL) to refine topologies, aiming to learn domain-invariant structural knowledge. To mitigate negative transfer, frameworks like GraphBridge (Ju et al. 2025) utilize a lightweight Mixture-of-Experts (MoE) network for selective knowledge transfer.

Despite these advances, most methods tackle feature and structure adaptation in isolation. For example, feature-centric models like MDGPT and BRIDGE may lack robustness to structural noise, while structure-focused approaches such as MDGFM can be computationally expensive. Furthermore, the interaction between semantic feature shifts and topological noise is often overlooked, preventing a holistic understanding of cross-domain generalization and robustness. This leaves a gap for a unified framework that motivates the design of our proposed method.

E.2 Robust Graph Representation Learning

Robust graph representation learning focuses on improving model stability under various forms of data uncertainty, including both feature and structural perturbations. To enhance semantic resilience against noise in node attributes, prior work has explored several strategies. These include data augmentation, which enriches training data through methods like intra-class mixup (Zheng, Wang, and Liu 2024) or learning beneficial noise (Huang et al. 2025); adversarial training on perturbed features to improve defensive capabilities (Lee and Park 2025); and disentangled learning, which separates invariant causal factors from spurious correlations to handle distribution shifts (Li et al. 2025).

On the structural level, research primarily addresses the vulnerability of GNNs to topological noise and adversarial attacks (Zügner, Akbarnejad, and Günnemann 2018). Graph Structure Learning (GSL) has emerged as a key defense strategy (Zhu et al. 2021), where the goal is to learn an optimized graph structure that is more reliable than the original input. Recent progress in this area includes techniques like topology-aware graph pruning, which removes potentially harmful edges to safeguard the model and improve its stability (Zhang et al. 2024).

However, a significant limitation of existing work is that feature and structure robustness are often treated as separate problems, without considering their interaction. Furthermore, many GSL approaches, including the one used in MDGFM, are computationally intensive and lack fine-grained control over distinct structural components such as intra- and inter-cluster connections. This gap for a more unified and efficient approach motivates our work.

E.3 Graph Structural Entropy

Graph Structural Entropy is an information-theoretic measure that quantifies the structural complexity of a network’s topology via an optimal encoding scheme (Li and Pan 2016). The theory posits that a graph’s structural information is the minimum number of bits needed to locate a node through a random walk. Minimizing this entropy yields a hierarchical encoding tree, which recursively partitions the graph to reveal its multi-scale community structure.

The hierarchical organization derived from structural entropy has been recognized as a valuable prior for graph representation learning. For instance, researchers have leveraged this principle to inject topic-aware signals into graph learning (Long et al. 2020) or to guide hierarchical clustering for learning more structurally informed node embeddings (Bai et al. 2024). These approaches validate the effectiveness of structural entropy in capturing meaningful topological patterns.

Despite its theoretical elegance, the potential of this hierarchical prior to systematically enhance raw node features for improving the robustness of Graph Foundation Models (GFMs) is largely untapped. Our work aims to fill this void, utilizing the encoding tree not merely as a structural summary, but as a direct source for generating structure-aware semantic augmentations to bolster model resilience against perturbations.

F Limitations

While SA²GFM shows promising results, there are several directions for future enhancement. Our robustness evaluation, while comprehensive, primarily centers on standard perturbations to node features and graph structures. A natural and important extension would be to test the model’s resilience against a wider range of adversarial scenarios, such as more complex topological attacks. This would provide a more complete picture of its defensive capabilities. Secondly, the framework’s effectiveness has been validated on benchmark homogeneous and static graphs. An important next step is to investigate its applicability to more complex graph types, such as large-scale heterogeneous or dynamic networks. Adapting the model for these scenarios is crucial for its practical deployment and represents a key area for future research. Finally, the current work focuses on establishing the core methodology of SA²GFM. Exploring its integration and potential synergies with other emerging pre-training paradigms is a promising avenue. Understanding how to combine our structure-aware approach with complementary techniques could lead to more powerful models.